

## Unveiling the Kondo cloud: Unitary renormalization-group study of the Kondo model

Anirban Mukherjee,<sup>1,\*</sup> Abhirup Mukherjee<sup>1,†</sup>, N. S. Vidhyadhiraja<sup>2,‡</sup>, A. Taraphder<sup>3,§</sup> and Siddhartha Lal<sup>1,||</sup>

<sup>1</sup>Department of Physical Sciences, Indian Institute of Science Education and Research-Kolkata, Mohanpur, West Bengal 741246, India

<sup>2</sup>Theoretical Sciences Unit, Jawaharlal Nehru Center for Advanced Scientific Research, Jakkur, Bengaluru 560064, India

<sup>3</sup>Department of Physics, Indian Institute of Technology Kharagpur, Kharagpur 721302, India



(Received 21 November 2021; revised 4 January 2022; accepted 31 January 2022; published 14 February 2022)

We analyze the single-channel Kondo model using the recently developed unitary renormalization-group (URG) method and obtain a comprehensive understanding of the Kondo screening cloud. The fixed-point low-energy Hamiltonian enables the computation of a plethora of thermodynamic quantities (specific heat, susceptibility, Wilson ratio, etc.) as well as spectral functions, all of which are found to be in good agreement with known results. By integrating out the impurity, we obtain an effective Hamiltonian for the excitations of the electrons comprising the Kondo cloud. This is found to contain both  $k$ -space number diagonal (Fermi liquid) and off-diagonal four-fermion scattering terms. Our conclusions are reinforced by a URG study of the two-particle entanglement and many-body correlations among members of the Kondo cloud and impurity. The entanglement between the impurity and a cloud electron, as well as between any two cloud electrons, is found to increase under flow towards the singlet ground state at the strong-coupling fixed point. Both the number diagonal and off-diagonal correlations within the conduction cloud are also found to increase as the impurity is screened under the flow, and the latter are found to be responsible for the macroscopic entanglement of the Kondo-singlet ground state. The URG flow enables an analytic computation of the phase shifts suffered by the conduction electrons at the strong-coupling fixed point. This reveals an orthogonality catastrophe between the local-moment and strong-coupling ground states and is related to a change in the Luttinger volume of the conduction bath under the crossover to strong coupling. Our results offer fresh insight into the nature of the emergent many-particle entanglement within the Kondo cloud and pave the way for further investigations in more exotic contexts such as the fixed point of the overscreened multichannel Kondo problem.

DOI: [10.1103/PhysRevB.105.085119](https://doi.org/10.1103/PhysRevB.105.085119)

### I. INTRODUCTION

In this paper, we present a unitary renormalization-group (URG) analysis of the single-channel Kondo model. The model involves a quantum impurity interacting with a conduction bath. It can be derived from the particle-hole-symmetric single-impurity Anderson model using a Schrieffer-Wolff transformation that integrates out single-particle interactions [1]. The model was initially developed to study metals with magnetic impurities and was used by Kondo [2,3] to explain the resistivity minimum that appears in these materials at low temperatures. Since then, various methods have been applied to determine the low-energy behavior of this model. Notable attempts include the Coulomb gas approach by Anderson and Yuval [4] and Anderson *et al.* [5] and perturbative renormalization-group approach (poor man's scaling) by Anderson [6]. The latter method showed that the Kondo exchange coupling  $J$  flows to larger values as we go to lower energy scales, at least for small  $J$ . The full crossover from the

local-moment phase at small  $J$  to the screened moment strong-coupling phase at large  $J$  was later obtained by the numerical renormalization-group (NRG) technique developed by Wilson [7,8], the Bethe ansatz solution by Andrei *et al.* [9] and Tsvetick and Wiegmann [10], and the conformal field theory (CFT) approach [11,12]. Another important strong-coupling approach based on arguments of scattering phase shifts is that of the local Fermi liquid theory [13,14] by Nozières. The low-temperature properties were found to be universal functions of a single energy scale, the Kondo temperature  $T_K$  [7,15–18]. All the predicted aspects of the Kondo effect, including the existence of the Kondo cloud [19–23], were observed experimentally in quantum dot systems [24–28]. Scanning tunneling spectroscopy (STS) measurements have revealed that the Kondo effect often depends on the neighborhood of the impurities, in Cu and Co atoms [29,30]. It was also shown [31], using quantum dots, that the out-of-equilibrium Kondo effect also displays universality, the physics at low temperatures being decided by only two energy scales, the frequency and amplitude of the perturbation. The impurity spectral function has been calculated using NRG [32], both at  $T = 0$  [33,34] and at  $T > 0$  [35], as well as using diagrammatic methods [36]. The electrical resistivity was found to obey single-parameter scaling behavior in  $T/T_K$  [37]. Nozières went further and analyzed a more realistic model, the multichannel Kondo problem, in which multiple conduction

\* mukherjee.anirban.anirban@gmail.com

† am18ip014@iiserkol.ac.in

‡ raja@jncasr.ac.in

§ arghya@phy.iitkgp.ernet.in

|| slal@iiserkol.ac.in

bath channels interact with quantum impurity at the center [38]. Such a model was found, through methods such as the Bethe ansatz, CFT, and bosonization, among others, to host a non-Fermi-liquid low-energy phase [38–49]. The Kondo effect also occurs in light quark matter which interacts with heavy quark impurities through gluon-exchange interactions; the scattering amplitude goes through a similar logarithmic divergence, and renormalization-group calculations reveal a Kondo scale in such systems [50,51]. The Kondo effect can also be realized for other fermionic systems such as graphene [52], Dirac-Weyl semimetals [53,54], and dense nuclear matter [50,55,56].

Obtaining the form of the effective Hamiltonian governing the low-energy physics of the Kondo cloud and the many-body singlet wave function has remained a challenge. In this paper, we have analyzed the Kondo model on a tight-binding lattice using the recently developed URG method [57,58]. This method has already been applied to a variety of problems such as the two-dimensional (2D) Hubbard model [59,60], the quantum kagome antiferromagnet [61], a generalized model of electrons in two spatial dimensions with attractive U(1)-symmetric interactions [62], the 1D Hubbard model [63], and other generalized models of electrons with repulsive interactions with and without translation invariance [58]. The method involves applying unitary transformations [see Eq. (2)] on the Hamiltonian that decouple high-energy electrons, creating a family of unitarily connected Hamiltonians at progressively smaller energy scales. The decoupled electrons lose their quantum fluctuations in the process, becoming integrals of motion (IOMs). This program leads to one of the main results of this work: a unitarily transformed strong-coupling fixed-point Hamiltonian. It is from this fixed-point Hamiltonian that we obtain the effective Hamiltonian for the electrons that comprise the Kondo cloud, by integrating out the impurity. This effective Hamiltonian is found to contain both Fermi liquid (diagonal) and off-diagonal four-fermion interaction terms, shedding new light on the nature of the Kondo cloud and the interactions within. It is seen that the flow towards the strong-coupling fixed point is concomitant with the growth of these off-diagonal terms, and this picture is made clearer by the evolution of the spectral function calculated using the effective Hamiltonians. For the purposes of benchmarking, we have also computed several thermodynamic quantities (e.g., the impurity susceptibility, specific heat, Wilson ratio, etc.) from this effective theory. These are described in Appendix D and are found to be in good agreement with the results known from the literature.

Another important result of this work involves studies of the evolution of the macroscopic entanglement of the Kondo cloud with the impurity spin and the many-body correlations inside the Kondo cloud under renormalization towards strong coupling. Experimental studies of entanglement and correlations have been performed in double quantum dots [64]. For the purpose of studying the entanglement and many-body correlations, we employ the entanglement renormalization-group (RG) method developed recently by some of us in Refs. [62,63,65]. These calculations are enabled by the fact that the RG transformations are unitary and preserve the total spectral weight. Thus iterative applications of the inverse of these unitary transformations on the IR fixed-point singlet

wave function generate a family of wave functions under a reversal of the RG flow towards the UV. The entanglement and correlation measures are then calculated from this family of wave functions and represent their RG evolution. The correlations (diagonal and off-diagonal) as well as the mutual information (among members of the cloud as well as between the impurity and the cloud) are found to increase towards the strong-coupling fixed point, and this is consistent with the presence of the off-diagonal scattering term which generates the correlation among the members of the cloud. Our quantification of the many-particle entanglement through the mutual information of the Kondo screening cloud and the impurity and the study of its renormalization is complementary to methods that have been used previously in the literature. This includes the impurity contribution to the entanglement of a region in the conduction bath (dubbed the impurity entanglement entropy in Refs. [66–68]), the entanglement entropy obtained by tracing out the impurity [19,69,70], and the concurrence between the impurity and the rest of the conduction bath [71]. Recent works have also shown, using negativity as a measure of entanglement [72], that the impurity is maximally entangled with the cloud [73].

The rest of the paper is outlined as follows. In Sec. II, we introduce the Hamiltonian for the single-channel Kondo model. We perform the URG analysis on the Hamiltonian in Sec. III. Section IV constitutes results on the scaling of the Kondo coupling, description of the low-energy stable fixed point in terms of the effective Hamiltonian and ground-state wave function, and the redistribution of spectral weight under the RG flow. In Sec. V, we obtain the effective Hamiltonian for the Kondo cloud excitations and describe the salient features. In Sec. VI, we study the entanglement features and many-body correlations of the Kondo cloud. We end in Sec. VII with a discussion of the results and some avenues for future investigations. Appendix A shows the derivation of the RG equation using the URG method. In Appendixes B and C, we obtain a real-space effective Hamiltonian for the low-energy excitations of the strong-coupling fixed-point Hamiltonian and calculate the conduction electron scattering phase shifts close to the ground state. Appendixes D 1 and D 2 focus on calculating some thermodynamic quantities (impurity susceptibility, impurity specific heat, and impurity thermal entropy) in order to benchmark with existing results.

## II. THE MODEL

The Kondo model [2,6] describes the coupling between a magnetic quantum impurity localized in real space and a bath of conduction electrons

$$\hat{H} = \sum_{\mathbf{k}\sigma} \epsilon_{\mathbf{k}} \hat{n}_{\mathbf{k}\sigma} + \frac{J}{2} \sum_{\mathbf{k}, \mathbf{k}'} \mathbf{S} \cdot c_{\mathbf{k}\sigma}^\dagger \boldsymbol{\sigma}_{\alpha\beta} c_{\mathbf{k}'\beta}. \quad (1)$$

We will consider a 2D electronic bath with a dispersion  $\epsilon_{\mathbf{k}} = -2t(\cos k_x + \cos k_y)$  and with the Fermi energy set to  $E_F = \mu$ . Here,  $J$  is the Kondo scattering coupling between the impurity and the conduction electrons. An important feature of the Kondo coupling is the two different classes of scattering processes: one involving spin-flip scattering processes for the

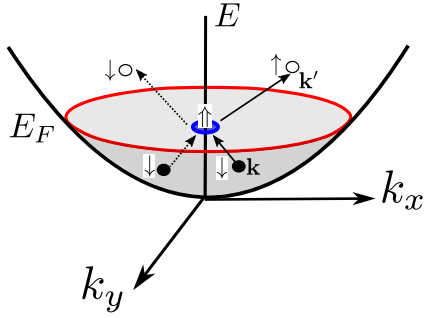


FIG. 1. The Kondo model is composed of a two-dimensional conduction electron bath (Fermi liquid) coupled to a magnetic impurity via a coupling of spin-flip scattering (solid arrows) and non-spin-flip scattering (dashed arrows).

bath electrons ( $c_{\mathbf{k}\uparrow}^\dagger c_{\mathbf{k}\downarrow} + \text{H.c.}$ ), and the other involving non-spin-flip (i.e., simple potential) scattering processes (Fig. 1). In the antiferromagnetic regime  $J > 0$ , the spin-flip scattering processes generate quantum entanglement between the impurity spin and a macroscopic number of bath electrons (called the “Kondo cloud”), resulting in the complete screening of the impurity via the formation of a singlet spin state. It is clear that the dynamical Kondo cloud corresponds to an effective single spin-1/2, such that the screening is an example of macroscopic quantum entanglement arising from electronic correlations. It is the nature of this entanglement, and the underlying quantum liquid that forms the Kondo cloud, that we seek to learn more of.

### III. URG THEORY FOR THE KONDO MODEL

In constructing an effective low-energy theory for the Kondo singlet, we apply the unitary RG formalism [57–63] to the Kondo model such that electronic states from the non-interacting conduction bath are stepwise disentangled, starting with the highest-energy electrons at the bandwidth and eventually scaling towards the Fermi surface (FS). While this aspect is similar to Anderson’s poor man’s scaling [6], we shall see that several other aspects of the unitary RG formalism are different from those adopted in the poor man’s scaling approach.

The electronic states are labeled in terms of the normal distance  $\Lambda$  from the FS and the orientation unit vectors  $\hat{s}$  (Fig. 2):  $\mathbf{k}_{\Lambda\hat{s}} = \mathbf{k}_F(\hat{s}) + \Lambda\hat{s}$ , where  $\hat{s} = \frac{\nabla_{\mathbf{k}} \epsilon_{\mathbf{k}}}{|\nabla_{\mathbf{k}} \epsilon_{\mathbf{k}}|} |_{\epsilon_{\mathbf{k}}=E_F}$ . The various  $\hat{s}$  represent the normal directions of the Fermi surface. The states are labeled as  $|j, l, \sigma\rangle = |\mathbf{k}_{\Lambda\hat{s}}, \sigma\rangle$ ,  $l := (\hat{s}_m, \sigma)$ . The  $\Lambda$ ’s are arranged as follows:  $\Lambda_N > \Lambda_{N-1} > \dots > 0$ , where the electronic states farthest from FS  $\Lambda_N$  are disentangled first, eventually scaling towards the FS. This leads to the Hamiltonian flow equation [57]

$$H_{(j-1)} = U_{(j)} H_{(j)} U_{(j)}^\dagger, \quad (2)$$

where the unitary operation  $U_{(j)}$  is the unitary map at RG step  $j$ .

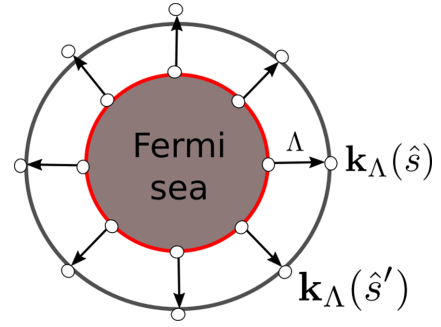


FIG. 2. Fermi surface geometry for a circular Fermi volume of noninteracting electrons in two spatial dimensions.

$U_{(j)}$  disentangles all the electronic states  $|\mathbf{k}_{\Lambda_j \hat{s}_m}, \sigma\rangle$  on the isogeometric curve and has the form [57,59]

$$U_{(j)} = \prod_l U_{j,l}, \quad U_{j,l} = \frac{1}{\sqrt{2}} [1 + \eta_{j,l} - \eta_{j,l}^\dagger], \quad (3)$$

where  $\eta_{j,l}$  are electron-hole transition operators following the algebra

$$\{\eta_{j,l}, \eta_{j,l}^\dagger\} = 1, \quad [\eta_{j,l}, \eta_{j,l}^\dagger] = 1. \quad (4)$$

The transition operator can be represented in terms of the diagonal ( $H^D$ ) and off-diagonal ( $H^X$ ) parts of the Hamiltonian as follows:

$$\eta_{j,l} = \text{Tr}_{j,l}(c_{j,l}^\dagger H_{j,l} c_{j,l}) \frac{1}{\hat{\omega}_{j,l} - \text{Tr}_{j,l}(H_{j,l}^D \hat{n}_{j,l}) \hat{n}_{j,l}}. \quad (5)$$

We note that in the numerator of the expression for  $\eta_{j,l}$ , the operator  $\text{Tr}_{j,l}(c_{j,l}^\dagger H_{j,l} c_{j,l}) + \text{H.c.}$  is composed of all possible scattering vertices that modify the configuration of the electronic state  $|j, l\rangle$  [57]. The generic forms of  $H_{j,l}^D$  and  $H_{j,l}^X$  are as follows:

$$H_{j,l}^D = \sum_{\Lambda, \hat{s}, \sigma} \epsilon^{j,l} \hat{n}_{\mathbf{k}_{\Lambda\hat{s}}, \sigma} + \sum_{\alpha} \Gamma_{\alpha}^{4, (j,l)} \hat{n}_{\mathbf{k}\sigma} \hat{n}_{\mathbf{k}'\sigma'} + \sum_{\beta} \Gamma_{\beta}^{8, (j,l)} \hat{n}_{\mathbf{k}\sigma} \hat{n}_{\mathbf{k}'\sigma'} (1 - \hat{n}_{\mathbf{k}''\sigma''}) + \dots, \quad (6)$$

$$H_{j,l}^X = \sum_{\alpha} \Gamma_{\alpha}^2 c_{\mathbf{k}\sigma}^\dagger c_{\mathbf{k}'\sigma'} + \sum_{\beta} \Gamma_{\beta}^2 c_{\mathbf{k}\sigma}^\dagger c_{\mathbf{k}'\sigma'} c_{\mathbf{k}_1\sigma_1}^\dagger c_{\mathbf{k}_1\sigma_1} + \dots$$

The indices  $\alpha$  and  $\beta$  are strings that denote the quantum numbers of the incoming and outgoing electronic states at a particular interaction vertex  $\Gamma_{\alpha}^n$  or  $\Gamma_{\beta}^m$ . The operator  $\hat{\omega}_{j,l}$  accounts for the quantum fluctuations arising from the non-commutation between different parts of the renormalized Hamiltonian and has the following form [57]:

$$\hat{\omega}_{j,l} = H_{j,l}^D + H_{j,l}^X - H_{j,l-1}^X. \quad (7)$$

Upon disentangling electronic states  $\hat{s}, \sigma$  along an isogeometric curve at distance  $\Lambda_j$ , the following effective Hamiltonian  $H_{j,l}$  is generated:

$$H_{j,l} = \prod_{m=1}^l U_{j,m} H_{(j)} \left[ \prod_{m=1}^l U_{j,m} \right]^\dagger. \quad (8)$$

Here,  $\tau_{j,l} = n_{j,l} - \frac{1}{2}$ . We note that  $H_{j,2n_j+1} = H_{(j-1)}$  is the Hamiltonian obtained after disentangling all  $2n_j$  electronic states on the isogeometric curve  $j$  at distance  $\Lambda_j$ . Below, we depict the different terms generated upon successive disentanglement of the states  $|\mathbf{k}_{\Lambda_j \hat{s}}, \sigma\rangle$  on a given curve,

$$\begin{aligned} H_{j,l+1} &= \text{Tr}_{j,l}(H_{(j,l)}) + \{c_{j,l}^\dagger \text{Tr}_{j,l}(H_{(j,l)}c_{j,l}), \eta_{j,l}\} \tau_{j,l}, \tau_{j,l} \\ &= \hat{n}_{j,l} - \frac{1}{2}, \\ H_{j,l+2} &= \text{Tr}_{j,l+1}(\text{Tr}_{j,l}(H_{(j,l)})) \\ &\quad + \text{Tr}_{j,l+1}(\{c_{j,l}^\dagger \text{Tr}_{j,l}(H_{(j,l)}c_{j,l}), \eta_{j,l}\} \tau_{j,l}) \\ &\quad + \{c_{j,l+1}^\dagger \text{Tr}_{j,l+1}(\text{Tr}_{j,l}(H_{(j,l)}c_{j,l+1})), \eta_{j,l+1}\} \tau_{j,l+1} \\ &\quad + \{c_{j,l+1}^\dagger \text{Tr}_{j,l+1}(\{c_{j,l}^\dagger \text{Tr}_{j,l}(H_{(j,l)}c_{j,l}), \eta_{j,l}\} c_{j,l+1}), \\ &\quad \times \eta_{j,l+1}\} \tau_{j,l} \tau_{j,l+1}, \\ H_{j,l+3} &= \dots \text{ terms with } \tau_{j,l}, \tau_{j,l+1}, \tau_{j,l+2} \dots \\ &\quad + \dots \text{ terms with } \tau_{j,l} \tau_{j,l+1}, \tau_{j,l+1} \tau_{j,l+2}, \tau_{j,l} \tau_{j,l+2} \dots \\ &\quad + \dots \text{ terms with } \tau_{j,l} \tau_{j,l+1} \tau_{j,l+2}. \end{aligned} \quad (9)$$

Upon disentangling, the multiple electronic states placed in the tangential direction on a given momentum shell at distance  $\Lambda_j$  generate a RG contribution from leading-order scattering processes (terms multiplied by  $\tau_{j,l}, \tau_{j,l+1}$  etc.) that scale as Area/Vol =  $1/L$ . Contributions from higher-order processes, such as terms multiplied by  $\tau_{j,l} \tau_{j,l+1}$  and  $\tau_{j,l} \tau_{j,l+1} \tau_{j,l+2}$ , scale as (Area)<sup>2</sup>/Vol<sup>2</sup> =  $1/L^2$  and (Area)<sup>3</sup>/Vol<sup>3</sup> =  $1/L^3$  respectively. Here, each factor of area arises from decoupling an entire shell of single-particle states ( $\tau_{j,l}$ ) at every RG step, and every factor of volume arises from the Kondo coupling. Accounting for only the leading tangential scattering processes, as well as other momentum transfer processes along the normal direction  $\hat{s}$ , the renormalized Hamiltonian  $H_{(j-1)}$  has the form [57]

$$\text{Tr}_{j,(1,\dots,2n_j)}(H_{(j)}) + \sum_{l=1}^{2n_j} \{c_{j,l}^\dagger \text{Tr}_{j,l}(H_{(j)}c_{j,l}), \eta_{j,l}\} \tau_{j,l}. \quad (10)$$

From the effective Hamiltonian obtained at the stable fixed point  $\hat{H}^*$ , we can compute the (un-normalized) density matrix operator ( $\hat{\rho} = e^{-\beta \hat{H}^*}$ ) and thence the finite-temperature partition function as

$$Z = \text{Tr}[\hat{\rho}] = \text{Tr}[e^{-\beta \hat{H}^*}] = \text{Tr}[U^\dagger e^{-\beta \hat{H}^*} U] = \text{Tr}[e^{-\beta \hat{H}}], \quad (11)$$

where  $\beta = 1/k_B T$ ,  $U = \prod_1^{j^*} U_{(j)}$ ,  $H$  is the bare Hamiltonian, and  $j^*$  is the RG step at which the IR stable fixed point is reached. This indicates that the partition function is preserved along the RG flow as the unitary transformations preserve the eigenspectrum.

#### IV. CROSSOVER FROM LOCAL MOMENT TO STRONG COUPLING

##### A. The ir fixed-point Hamiltonian and wave function

The unitary RG process generates the effective Hamiltonian's  $\hat{H}_{(j)}(\omega)$ 's for various eigendirections  $|\Phi(\omega)\rangle$  of the  $\hat{\omega}$  operator. Note that the associated eigenvalue  $\omega$  identifies a subspectrum in the interacting many-body eigenspace. The

form of  $\hat{H}_{(j)}(\omega)$  is given by

$$\sum_{j,l,\sigma} \epsilon_{j,l} \hat{n}_{j,l} + J^{(j)}(\omega) \mathbf{S} \cdot \mathbf{s}_< + \sum_{\substack{a=N, \\ m=1}}^{j,n_j} J^{(a)} S^z s_{a,\hat{s},m}^z, \quad (12)$$

where the label  $a$  indexes the isoenergetic shells that have already been decoupled and hence run from the furthest shell  $a = N$  to the most recently decoupled shell  $a = j$ . We also defined  $\mathbf{s}_< = \frac{1}{2} \sum_{\substack{j_1, j_2 < j^*, \\ m, m'}} c_{j_1, \hat{s}_m, \alpha}^\dagger \boldsymbol{\sigma}_{\alpha\beta} c_{j_2, \hat{s}_{m'}, \beta}$  as the total

spin operator for the Kondo cloud and  $s_{l,\hat{s},m}^z = \frac{1}{2}(\hat{n}_{l,\hat{s}_m,\uparrow} - \hat{n}_{l,\hat{s}_m,\downarrow})$ . The derivation of the above equation is presented in Appendix A. Here, the second term is the effective Hamiltonian for the coupling of the Kondo cloud to the impurity spin, while the third encodes the interaction between the impurity spin moment and the decoupled electronic degrees of freedom that do not belong to the Kondo cloud (lying on radial shells in momentum space indexed by the RG step  $j$ ). Note that the third term is an Ising coupling and involves only potential scattering of the decoupled electrons and the impurity; hence it does not cause any spin-flip scattering of the impurity spin. Importantly, we will see later that Eq. (12) encodes the entire  $T = 0$  RG crossover. Employing Eq. (11), this enables a computation of the entire RG crossover at finite  $T$  as well. The Kondo coupling RG equation for the RG steps (Appendix A) has the form

$$\frac{\Delta J^{(j)}(\omega)}{\Delta \ln \frac{\Lambda_j}{\Lambda_0}} = \frac{n_j (J^{(j)})^2 \left[ \left( \omega - \frac{\hbar v_F \Lambda_j}{2} \right) \right]}{\left( \omega - \frac{\hbar v_F \Lambda_j}{2} \right)^2 - \frac{(J^{(j)})^2}{16}}, \quad (13)$$

where  $n_j = \sum_{\hat{s}} 1$  is the number of states on the isogeometric shell at distance  $\Lambda_j$  from the Fermi surface. We have assumed that the conduction bath dispersion is linear near the Fermi surface:  $\epsilon_j = \hbar v_F \Lambda_j$ ,  $v_F$  being the Fermi velocity. Note that the denominator  $\Delta \ln \frac{\Lambda_j}{\Lambda_0} = 1$  for the RG scale parametrization  $\Lambda_j = \Lambda_0 \exp(-j)$ . We now redefine Kondo coupling as a dimensionless parameter

$$K^{(j)} = \frac{J^{(j)}}{\omega - \frac{\hbar v_F}{2} \Lambda_j} \quad (14)$$

and operate in the regime  $\omega > \frac{\hbar v_F}{2} \Lambda_j$ . With the above parametrization of Eq. (14), we can convert the difference RG relation [Eq. (13)] into a continuum RG equation

$$\frac{dK}{d \ln \frac{\Lambda}{\Lambda_0}} = \left( 1 - \frac{\omega}{\omega - \frac{1}{2} \hbar v_F \Lambda} \right) K + \frac{n(\Lambda) K^2}{1 - \frac{K^2}{16}}, \quad (15)$$

where  $n(\Lambda)$  is the continuum counterpart of  $n_j$  and represents the number of electronic states on the isogeometric shell at momentum  $\Lambda$ .

Upon approaching the Fermi surface,  $\Lambda_j \rightarrow 0$ ; hence  $(1 - \frac{\omega}{\omega - \hbar v_F \Lambda}) \rightarrow 0$ , and  $n(\Lambda)$  can be replaced by density of states on the Fermi surface  $n(0)$ :

$$\frac{dK}{d \ln \frac{\Lambda}{\Lambda_0}} = \frac{n(0) K^2}{1 - \frac{K^2}{16}}. \quad (16)$$

At this point, we observe an important aspect of the RG equation: For  $K \ll 1$ , the RG equation reduces to the one-loop form:  $\frac{dK}{d \ln \frac{\Lambda}{\Lambda_0}} = K^2$  [6]. On the other hand, the nonperturbative

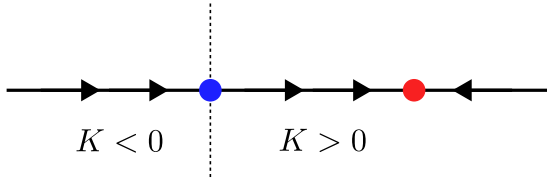


FIG. 3. Schematic RG phase diagram for the Kondo problem. The red dot represents the intermediate-coupling fixed point at  $K^* = 4$  for the case of the antiferromagnetic Kondo coupling. The blue dot represents the critical fixed point at  $K^* = 0$  for the case of the ferromagnetic Kondo coupling.

form of the flow equation obtained from the URG formalism shows the presence of an intermediate-coupling fixed point at  $K^* = 4$  in the antiferromagnetic regime  $K > 0$  (Figs. 3 and 4). Upon integrating the RG equation and using the fixed-point value  $K^* = 4$ , we obtain the Kondo energy scale ( $T_K$ ) and thence the effective length of the Kondo cloud ( $\xi_K$ )

$$\frac{1}{K_0} - \frac{1}{2} + \frac{K_0}{16} = -n(0) \ln \frac{\Lambda^*}{\Lambda_0}, \quad (17)$$

$$\Lambda^* = \Lambda_0 \exp\left(\frac{1}{2n(0)} - \frac{1}{n(0)K_0} - \frac{K_0}{n(0)16}\right), \quad (18)$$

$$T_K = \frac{\hbar v_F \Lambda_0}{k_B} \exp\left(\frac{1}{2n(0)} - \frac{1}{n(0)K_0} - \frac{K_0}{n(0)16}\right), \quad \xi_K = \frac{2\pi}{\Lambda^*}. \quad (19)$$

At the IR fixed point in the antiferromagnetic regime the effective Hamiltonian is given by

$$H^* = \sum_{|\Lambda| < \Lambda^*} \hbar v_F \Lambda \hat{n}_{\Lambda, \hat{s}, \sigma} + J^* \mathbf{S} \cdot \mathbf{s}_< + \sum_{j'=N, m=1}^{j^*, n_j} J^{j'} S^z s_{j', m}^z. \quad (20)$$

In the equation,  $m$  refers to the various normal directions  $\hat{s}_m$  of the Fermi surface. In the above equation, the second term is the effective Hamiltonian for the coupling of the Kondo cloud

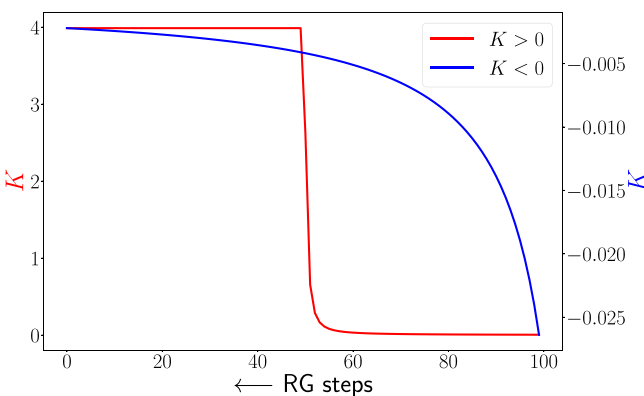


FIG. 4. Red: renormalization of the dimensionless Kondo coupling  $K$  towards the strong-coupling fixed point ( $K > 0$ ) with RG steps ( $\ln \Lambda_j / \Lambda_0$ ). The growth of the Kondo coupling to a finite value of the intermediate-coupling fixed point is evident. Blue: decay of the dimensionless Kondo coupling  $K$  to zero towards the local-moment critical fixed point ( $K < 0$ ) with RG steps ( $\ln \Lambda_j / \Lambda_0$ ). For these plots, we chose  $\omega = \hbar v_F \Lambda_j$ .

to the impurity spin. The third encodes the Ising interaction between the impurity spin moment and the magnetic moment of the decoupled electronic degrees of freedom that do not belong to the Kondo cloud (lying on radial shells in momentum space indexed by the RG step  $j$ , and corresponding to the IOMs generated during the RG flow). As reported in Appendix D, the fixed-point Hamiltonian has been used to compute various thermodynamic quantities such as the impurity susceptibility, impurity specific heat, thermal entropy, Wilson number, and Wilson ratio. The values obtained are found to be in good agreement with those from other methods such as the NRG or the Bethe ansatz [7, 8, 74, 75].

We can now extract a zero mode from the above Hamiltonian that captures the low-energy theory near the Fermi surface,

$$H_{\text{coll}} = \frac{1}{N} \sum_{|\Lambda| < \Lambda^*} \hbar v_F \Lambda \sum_{|\Lambda| < \Lambda^*} \hat{n}_{\Lambda, \hat{s}, \sigma} + J^* \mathbf{S} \cdot \mathbf{s}_< + \sum_{j'=N, m=1}^{j^*, n_j} J^{j'} S^z s_{j', m}^z = J^* \mathbf{S} \cdot \mathbf{s}_< + \sum_{j'=N, m=1}^{j^*, n_j} J^{j'} S^z s_{j', m}^z. \quad (21)$$

In the first step, the first term vanishes as the sum over wave vector  $\Lambda$  within the symmetric window  $\Lambda^*$  around the Fermi surface itself vanishes. Indeed, by taking the Ising coupling between the impurity spin and the IOMs ( $s_{j', m}^z$ ) to be a constant, we observe that the Kondo-singlet state

$$|\Psi^*\rangle = \frac{1}{\sqrt{2}} (|\uparrow_d, \downarrow\rangle \otimes |\downarrow\rangle - |\downarrow_d, \uparrow\rangle \otimes |\uparrow\rangle) \quad (22)$$

corresponds to the ground state of the zero-mode Hamiltonian at the IR fixed point [Eq. (21)]. In the singlet state written above,  $|\uparrow_d\rangle$  and  $|\downarrow_d\rangle$  represent the configuration of the impurity spin  $S^z$ ,  $|\uparrow\rangle$  and  $|\downarrow\rangle$  represent the configuration of the spin of the Kondo cloud  $s^z_<$ , and  $|\uparrow\rangle$  and  $|\downarrow\rangle$  represent the spin of the IOMs  $s^z = \sum_{j_1 > j^*} \hat{n}_{j_1, \hat{s}_m, \alpha} \sigma_{\alpha\beta}^z$ . Signatures of such a singlet ground state have been experimentally probed using nuclear magnetic resonance (NMR) experiments in Cu nuclei [76], using conductance measurements in carbon nanotubes [77–79], and using STS measurements in quantum corrals [80–83].

## B. Kondo cloud size and effective Kondo coupling as functions of bare coupling $J_0$

In Fig. 5, we show the variation of the Kondo cloud size  $\xi_K$  and effective Kondo coupling  $J^*$  as a function of bare coupling  $J$  (in units of  $t$ ) in the range  $5.7 \times 10^{-5} < J < 5.4$ . All plots below (including Fig. 5) are obtained for momentum-space grid  $100 \times 100$  and with RG scale factor  $\Lambda_j = b \Lambda_{j+1}$  ( $b = 0.9999 = 1 - 1/N^2$ ,  $N = 100$ ). The  $E_F$  for the 2D tight-binding band  $-W < E_k = -2t(\cos k_x + \cos k_y) < W$  ( $W = 4t$ ) is chosen at  $E_F = -3.9t$ , and the bare  $k$ -space cutoff is set at  $\Lambda_0 \simeq 2.83$ . The variation of the renormalized Kondo coupling  $J^*$  with the bare  $J$  shown in Fig. 5 clearly indicates the flow under RG towards saturation at a strong-coupling value

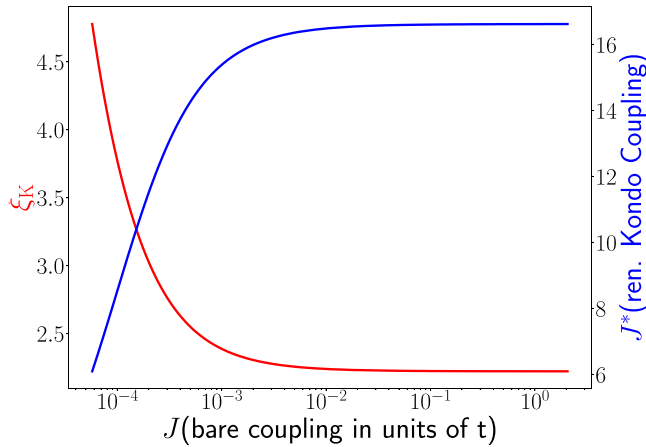


FIG. 5. Red: Kondo cloud length  $\xi_K$  vs bare Kondo coupling  $J$ . Blue: renormalized (ren.) Kondo coupling  $J^*$  vs  $J$  ( $x$  axis in log scale). The bare Kondo coupling  $J$  is chosen to lie within the range  $5.7 \times 10^{-5} < J < 5.4$ .

of  $J_{\text{sat}}^* \sim 16$ . Similarly, the variation of the Kondo screening length  $\xi_K$  with  $J$  in Fig. 5 shows a fall to an asymptotic value of  $\xi_K \sim 3$  lattice sites at the strong-coupling fixed point. We recall that Wilson's NRG calculation for the Kondo problem (for a bath of conduction electrons in the continuum with linear dispersion and a very large UV cutoff  $D$ ) shows that the renormalized Kondo coupling  $J^* \rightarrow \infty$  under flow to strong coupling. This can be reconciled with our URG results by noting that the value of  $J_{\text{sat}}^*$  increases upon rescaling the conduction bath bandwidth  $D$  to larger values (by rescaling the nearest-neighbor hopping strength  $t$ ). This is shown in Fig. 6, where we see that  $J_{\text{sat}}^*$  increases from a value of  $O(1)$  (in units of  $t$ ) to  $O(10^9)$  as  $t$  is increased from  $O(1)$  to  $O(10^4)$ . Thus taking the limit of  $D \rightarrow \infty$  will lead to  $J_{\text{sat}}^* \rightarrow \infty$ .

There is another aspect of this method that is worth pointing out: The size of the Kondo cloud emerges as a natural length scale of the low-energy theory. The URG moves forward by decoupling high-momentum states. Each momentum

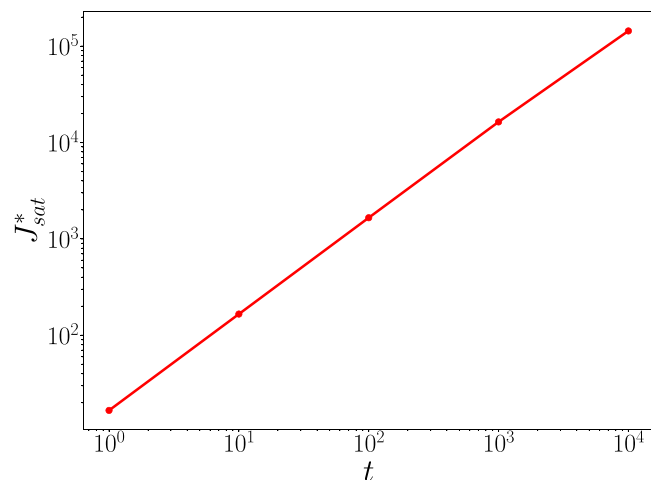


FIG. 6. Variation of the renormalized Kondo coupling  $J^*$  with the hopping parameter  $O(1) < t < O(10^4)$  of the electronic bath (and hence the bandwidth).

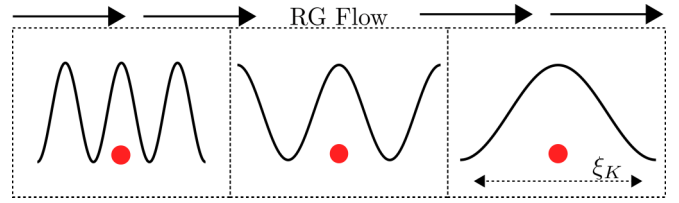


FIG. 7. Emergence of the Kondo length scale under URG. The red dot represents the impurity site, while the wavelike structure represents the shortest wavelength interacting with the impurity at any given point of the RG. The leftmost image is closest to the local-moment fixed point, while the rightmost image is closest to the strong-coupling one.

state wave function  $\Psi_k$  is associated with a de Broglie wavelength  $\lambda_k \sim \frac{1}{k}$ . At high energies (temperatures), all possible wavelengths are interacting with the impurity. Under RG, the shortest of these wavelengths get decoupled, and the impurity interacts with only longer wavelengths. The shortest such wavelength that is still interacting with the impurity at the fixed point defines the Kondo length scale  $\xi_K$  (Fig. 7).

The members of the Kondo cloud then involve all states with wavelengths starting from  $\xi_K$  and extending up to  $\infty$ . From existing results as well as our own investigations (inset of Fig. 8), it is clear that the width of the spectral function increases with temperature. This width defines the relevant energy scale  $\omega(T)$  [and hence a relevant length scale  $\xi(T) \sim \omega^{-1}(T)$ ] for interactions with the impurity. Higher temperatures therefore lead to reduced  $\xi(T)$ . This means that at sufficiently large temperatures, the relevant length scale  $\xi(T)$  is shorter than the Kondo length scale  $\xi_K$ :  $\xi(T) \ll \xi_K$ , which means that the Kondo effect will not manifest at temperatures  $T \gg T_K$ : The RG flow is not able to filter out the low-energy physics because of the thermal fluctuations. Similar insights were obtained in Ref. [84] using a real-space renormalization-group flow.

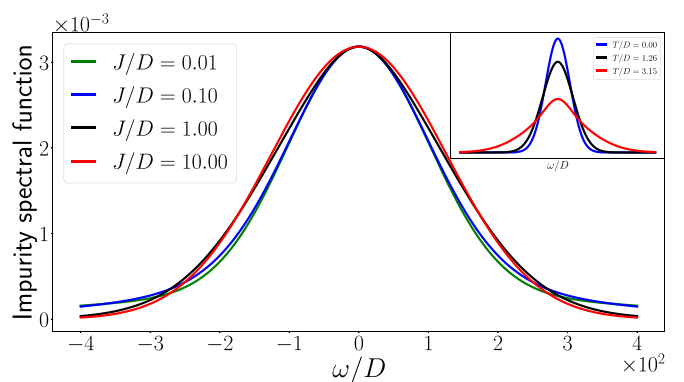


FIG. 8. Impurity spectral function as a function of  $\omega/D$  at various values of  $J$ , starting from weak coupling and extending up to strong coupling.  $D$  is the half bandwidth and is set to 1. The inset shows the spectral function at various temperatures. The width increases with increasing temperature (see final paragraph of Sec. IV B).

### C. Redistribution of spectral weight under RG flow

The presence of a unitarily transformed effective Hamiltonian at each stage of the RG allows one to map the journey in terms of changes in the distribution of the total spectral weight. In this section, we will compute the impurity spectral function at various values of the running coupling  $J$ , following the expression [85,86]

$$A_d^\sigma = -\frac{1}{\pi} \text{Im} \langle \{O_\sigma, O_\sigma^\dagger\} \rangle, \quad O_\sigma = \frac{J}{2} (S^{-\sigma} c_{0,-\sigma} + S^z c_{0,\sigma}), \quad (23)$$

where  $\langle \dots \rangle$  indicates a thermal average,  $\{, \}$  indicates an anticommutator, and  $c_{0,\sigma} = \sum_k c_{k\sigma}$ .

In order to plot the spectral function (Fig. 8), we chose various values of  $J$  to mimic the crossover from the local-moment to the strong-coupling fixed points. The spectral function is normalized by dividing by the total area under the curve. The evolution of the spectral functions shows the increase in the spectral weight at the zero-energy resonance at the cost of that at higher frequencies. This transfer of spectral weight occurs because the high-frequency excitations are slowly getting integrated out and consumed into the IOMs, while the Kondo cloud gets distilled into purely low-energy modes proximate to the Fermi surface. This should be contrasted with the sharpening of the Abrikosov-Suhl resonance in the spectral function of the bare Hamiltonian as obtained from other methods (e.g., NRG), which corresponds to the excitations of the local Fermi liquid.

The inset of Fig. 8 also shows the change in the spectral function when temperature is introduced. The broadening of the central peak implies a decrease in the relevant length scale and hence a destruction of screening for  $T \gg T_K$ . This was also shown in Ref. [85].

### V. EFFECTIVE HAMILTONIAN FOR EXCITATIONS OF THE KONDO CLOUD

In this section we will study the effect of the renormalized Kondo coupling on the self-energy of the electrons comprising the Kondo cloud. We integrate out the decoupled electronic states to obtain the effective Hamiltonian  $H^*$  of the impurity + electronic cloud system. In this Hamiltonian we have additionally kept the electronic dispersion to study the effect of electronic density fluctuation due to the interelectronic interaction mediated by the impurity spin,

$$H^* = H_0^* + \frac{J^*}{2} \sum_{\substack{j_1, j_2 < j^* \\ m, m'}} \mathbf{S} \cdot c_{j_1, \hat{s}_m, \alpha}^\dagger \sigma_{\alpha\beta} c_{j_2, \hat{s}_{m'}, \beta}, \quad (24)$$

where  $H_0^* = \sum_{|\Lambda_j| < \Lambda^*, \sigma} \epsilon_j \hat{n}_{j, \hat{s}, \sigma}$ . In order to study the interelectronic interaction, we need to isolate the quantum impurity from the Kondo cloud. This can be done by first recasting the many-body eigenstate  $|\Psi\rangle$  of  $H^*$  in the  $|\uparrow_d\rangle, |\downarrow_d\rangle$  basis of the impurity and the associated configuration of the rest of the electronic states. We will then perform a perturbative expansion in the small parameter  $\frac{J^2}{J}$ , from which we obtain the effective  $k$ -space Hamiltonian for the Kondo cloud. This is justified by the fact that the Kondo coupling can be

made arbitrarily large by performing the expansion as close to the strong-coupling fixed point as desired.

At the ground state, the wave function will be a singlet composed of the impurity spin and the composite spin formed by the conduction electrons at the origin ( $|\uparrow\rangle, |\downarrow\rangle$ ):  $|\Psi\rangle = a_0 |\uparrow_d\rangle |\downarrow\rangle + a_1 |\downarrow_d\rangle |\uparrow\rangle$ . With this ground state in mind, we can rewrite the eigenvalue relation  $H_K^* |\Psi\rangle = E_{\text{GS}} |\Psi\rangle$  as a set of two coupled equations:

$$\begin{aligned} a_0 \left( H_0^* + \frac{J^*}{2} s_z \right) |\downarrow\rangle + a_1 \frac{J^*}{2} s_- |\uparrow\rangle &= a_0 E_{\text{GS}} |\downarrow\rangle, \\ a_0 \frac{J^*}{2} s_+ |\downarrow\rangle + a_1 \left( H_0^* - \frac{J^*}{2} s_z \right) |\uparrow\rangle &= a_1 E_{\text{GS}} |\uparrow\rangle. \end{aligned} \quad (25)$$

By combining these two equations and eliminating  $|\uparrow\rangle$ , we obtain the effective Hamiltonian for excitations in the subspace of states  $|\downarrow\rangle$ :

$$\left[ H_0^* + \frac{J^*}{2} s_z + s_- \frac{\frac{(J^*)^2}{4}}{E_{\text{GS}} + \frac{J^*}{2} s_z - H_0^*} s_+ \right] |\downarrow\rangle = E_{\text{GS}} |\downarrow\rangle. \quad (26)$$

From here we obtain the form of the effective Hamiltonian accounting for the leading-order density-density and off-diagonal four-fermion interaction terms, by expanding the denominator in powers of  $H_0^*/J$ .

$$\begin{aligned} H_0^* + \frac{J^*}{2} s_z + s_- \frac{\frac{(J^*)^2}{4}}{\left( E_{\text{GS}} + \frac{J^*}{2} s_z \right) \left( 1 - \frac{1}{E_{\text{GS}} + \frac{J^*}{2} s_z} H_0^* \right)} s_+ \\ \approx H_0^* + \frac{J^*}{2} s_z + s_- \frac{\frac{(J^*)^2}{4}}{E_{\text{GS}} + \frac{J^*}{2} s_z} \left( 1 + \frac{1}{E_{\text{GS}} + \frac{J^*}{2} s_z} H_0^* \right. \\ \left. + \frac{1}{E_{\text{GS}} + \frac{J^*}{2} s_z} H_0^* \frac{1}{E_{\text{GS}} + \frac{J^*}{2} s_z} H_0^* \right) s_+ + O((H_0^*)^3) \\ \approx H_0^* + \frac{J^*}{2} s_z + s_- \frac{\frac{(J^*)^2}{4}}{E_{\text{GS}} + \frac{J^*}{2} s_z} s_+ + s_- \frac{\frac{(J^*)^2}{4}}{\left( E_{\text{GS}} + \frac{J^*}{2} s_z \right)^2} H_0^* s_+ \\ + s_- \frac{\frac{(J^*)^2}{4}}{\left( E_{\text{GS}} + \frac{J^*}{2} s_z \right)^2} H_0^* \frac{1}{E_{\text{GS}} + \frac{J^*}{2} s_z} H_0^* s_+ \\ \approx H_0^* + \frac{J^*}{2} s_z + \left( \frac{1}{2} - s_z \right) \frac{\frac{(J^*)^2}{4}}{E_{\text{GS}} + \frac{J^*}{4}} \\ + s_+ \frac{\frac{(J^*)^2}{4}}{\left( E_{\text{GS}} + \frac{J^*}{2} s_z \right)^2} (s_- H_0^* + [H_0^*, s_-]) \\ + s_+ \frac{\frac{(J^*)^2}{4}}{\left( E_{\text{GS}} + \frac{J^*}{2} s_z \right)^2} H_0^* \frac{1}{E_{\text{GS}} + \frac{J^*}{2} s_z} (s_- H_0^* + [H_0^*, s_-]). \end{aligned} \quad (27)$$

In the second and third terms, we can substitute  $s^z = -\frac{1}{2}$ , because  $s^z |\downarrow\rangle = -\frac{1}{2} |\downarrow\rangle$ . We will also substitute the singlet binding energy  $-\frac{3J^*}{4}$  as the ground-state energy  $E_{\text{GS}}$  because  $J \gg \epsilon_k$  at the strong-coupling fixed point, and  $H_0^* = E_0^*$  as the kinetic

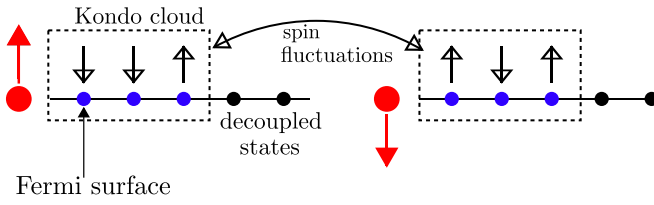


FIG. 9. The electronic Kondo cloud (dashed rectangle) coupled to the impurity spin (red dot and arrow). The blue dots represent momentum+spin states inside the Kondo cloud, while the black dots represent states outside the Kondo cloud (that is, among the IOMs). The ground-state singlet is formed by the impurity (red dot) and the Kondo cloud members (blue dots).

energy part of the ground state  $|\downarrow\rangle$ :

$$H_{\text{eff}} = -\frac{3J^*}{4} + E_0^* + s_+ \frac{\frac{(J^*)^2}{4}}{(E_{\text{GS}} + \frac{J^*}{2}s_z)^2} \left( s_- H_0^* + [H_0^*, s_-] \right. \\ \left. + H_0^* \frac{1}{E_{\text{GS}} + \frac{J^*}{2}s_z} (s_- H_0^* + [H_0^*, s_-]) \right). \quad (28)$$

This effective Hamiltonian has the expected structure; there are constant pieces that represent the diagonal part of the Hamiltonian, and then there are terms that scatter within the subspace. We will henceforth drop the constant terms and keep only the excitations within the subspace. After simplifying the terms and retaining at most four-fermion interactions, we obtain the following effective Hamiltonian:

$$H_{\text{eff}} = 2 \left( H_0^* + \frac{1}{J^*} H_0^{*2} \right) + \sum_{1234} V_{1234} c_{k_4\uparrow}^\dagger c_{k_3\downarrow}^\dagger c_{k_2\downarrow} c_{k_1\uparrow}, \quad (29)$$

where  $V_{1234} = (\epsilon_{k_1} - \epsilon_{k_3})[1 - \frac{2}{J^*}(\epsilon_{k_3} - \epsilon_{k_1} + \epsilon_{k_2} + \epsilon_{k_4})]$ . The first, second, and third terms represent a kinetic energy [see definition of  $H_0^*$  below Eq. (24)], a density-density correlation [see Eq. (D8) below], and a spin-fluctuation-mediated electron-electron scattering process, respectively. The presence of the off-diagonal scattering term is expected because the ground-state singlet is highly entangled and integrating out the impurity from this singlet should lead to scattering among the conduction electron states. In other words, it is this off-diagonal interaction that is a signal of the strongly screened local moment.

## VI. MANY-BODY CORRELATIONS AND ENTANGLEMENT PROPERTIES OF THE KONDO CLOUD

In order to study the effect of the off-diagonal terms [Eq. (29)] on the constituents of the Kondo cloud, we perform a reverse URG treatment (shown in Fig. 10) starting from the Kondo model ground state  $|\Psi^*\rangle$  at the IR fixed point [Eq. (22)]. For this, we employ the entanglement RG method developed recently by some of us in Refs. [62,63,65]. For the present study we take a toy model construction of the ground-state wave function  $|\Psi^*\rangle$  [Eq. (22)] at the IR fixed point; the Kondo impurity couples to 12 electronic states  $|\mathbf{k}\sigma\rangle$ , of which three are occupied and nine are unoccupied. The net spin of the electrons comprising the Kondo cloud is oppositely aligned to that of the Kondo impurity. The Kondo cloud system is a tensor product with 14 separable electronic states.

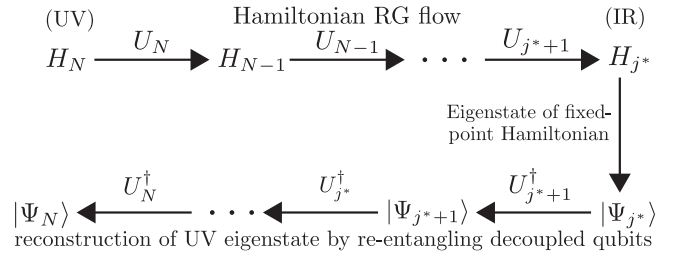


FIG. 10. The upper row represents the Hamiltonian RG flow via the unitary maps, while the lower row represents the reverse RG flow on the ground-state wave function obtained at the Kondo IR fixed point. The reverse RG reentangles decoupled electronic states with the Kondo singlet. This will result in generation of the many-body eigenstates at UV scales.

This construction is represented in Fig. 9. At each URG step  $U_{j,\uparrow}U_{j,\downarrow}$ , two electronic states  $|k_j, \uparrow\rangle, |k_j, \downarrow\rangle$  are disentangled in reaching the IR fixed point. Upon performing reverse RG, at each step two electrons are reentangled into the eigenstates via the inverse unitary maps  $U_{j,\uparrow}^\dagger U_{j,\downarrow}^\dagger$  (Fig. 10); in total we perform seven reverse RG steps. This reverse RG program is numerically implemented using PYTHON. Since the forward RG is driven by the unitary transformation  $U = \frac{1}{\sqrt{2}}(1 + \eta - \eta^\dagger)$ , the inverse transformation is  $\frac{1}{\sqrt{2}}(1 - \eta + \eta^\dagger)$ . The  $\eta$  have already been described in Appendix A. The inverse transformation for reentangling an electron of spin  $\sigma$  and energy  $\epsilon_q$  can therefore be written as

$$U_{q\sigma}^{-1} = \frac{1}{\sqrt{2}} \left[ 1 - \frac{J^2}{2} \frac{1}{2\omega\tau_{q\sigma} - \epsilon_q\tau_{q\sigma} - JS^z s_q^z} (\hat{O} + \hat{O}^\dagger) \right], \quad (30)$$

where  $\hat{O} = \sum_{k<\Lambda^*} \sum_{\alpha=\uparrow,\downarrow} \sum_{a=x,y,z} S^a \sigma_{\alpha\sigma}^\dagger c_{k\alpha}^\dagger c_{q\sigma}$ . The wave functions for the reverse RG are generated by repeat application of this inverse unitary operator on the fixed-point ground-state  $|\Psi^*\rangle$ . The total operator to reentangle the energy states  $\epsilon_{q_1}, \epsilon_{q_2}, \dots, \epsilon_{q_N}$  is

$$|\Psi_j\rangle = \prod_{q=q_1}^{q_N} U_{q\uparrow}^{-1} U_{q\downarrow}^{-1} |\Psi^*\rangle. \quad (31)$$

We use the wave functions generated under the reverse RG to compute the mutual information between (a) an electron in the Kondo cloud and the impurity electron and (b) two electrons within the cloud. The mutual information (MI) measures the total amount of quantum and classical correlations in a system [87]. The MI between two electrons is given by

$$I(i : j) = -\text{Tr}(\rho_i \ln \rho_i) - \text{Tr}(\rho_j \ln \rho_j) + \text{Tr}(\rho_{ij} \ln \rho_{ij}), \quad (32)$$

where  $\rho_i$  or  $\rho_j$  and  $\rho_{ij}$  are the one- and two-electron reduced density matrices, respectively, obtained from the wave functions obtained at each step of the reverse RG simulation. In Fig. 11, we present the RG flow of both types of mutual information mentioned above. The red curve in the top panel of Fig. 11 represents the plot for the maximum mutual information  $I(e : e)$  [Eq. (32)] between any two of the electrons comprising the Kondo cloud and shows that the maximum entanglement content or quantum correlation increases under RG flow from UV to IR. This implies that the

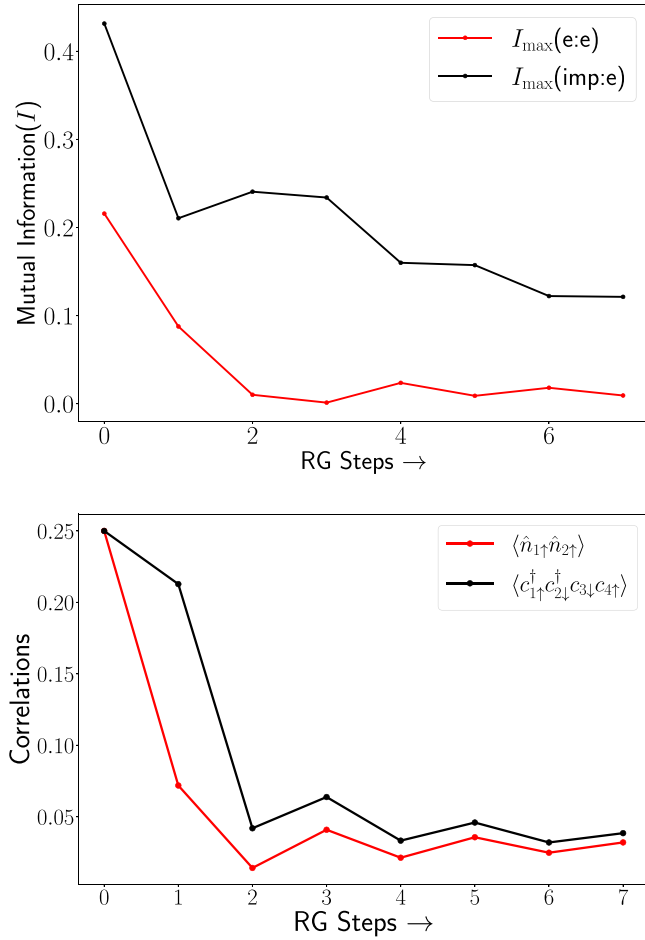


FIG. 11. Top: the RG flows for the maximum mutual information between the impurity (imp) and electron (black curve) and diagonal correlations (red curve). Bottom: the RG flows for the off-diagonal (black curve) and diagonal correlations (red curve).

electrons within the Kondo cloud are not simply a separable state in momentum space as expected of a local Fermi liquid. This is a strong indication of the fact that the two-particle off-diagonal ( $c_{k_4\uparrow}^\dagger c_{k_1\downarrow}^\dagger c_{k_2\downarrow} c_{k_3\uparrow}$ ) scattering term in Eq. (29) is playing a role in the electronic entanglement within the Kondo cloud. Furthermore, the black curve in the top panel of Fig. 11 shows that the maximum mutual information between the Kondo impurity and any one member of the electronic cloud also increases under RG and to a higher value compared with that between electrons. This originates from the maximally entangled singlet state that is formed between the impurity and the electronic cloud (as can also be observed from the  $\ln 2$  entanglement entropy obtained by tracing out the impurity spin from the singlet state). In this manner, the Kondo impurity mediates the entanglement between electrons (red curve) in the Kondo cloud.

In order to understand this further, we also study (i) the maximum density-density correlations  $\max_{k,k_1} \langle \hat{n}_{k\uparrow} \hat{n}_{k_1\downarrow} \rangle$  [red curve in the bottom panel of Fig. 11] and (ii) the maximum two-particle off-diagonal correlations  $\max_{k,k_1} \langle c_{k\uparrow}^\dagger c_{k_1\downarrow}^\dagger c_{k_2\downarrow} c_{k_3\uparrow} \rangle$  [black curve in the bottom panel of Fig. 11] between electrons within the Kondo cloud. The plots show clearly that both the correlations grow under RG

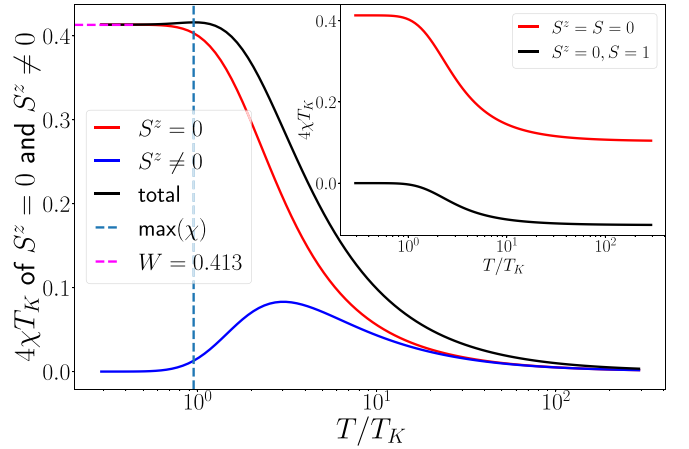


FIG. 12. Variation of  $4T_K \chi$  with  $T/T_K$ , for individual spin subspaces as well as the total.  $T_K$  corresponds to the Kondo temperature. The inset shows the difference in the contributions to  $\chi$  coming from the singlet and the triplet zero states. The dashed line shows the maximum in  $\chi$  and passes through  $T_K$ .

from UV to IR, finally reach the same value at the IR fixed point. On the other hand, the large values of the off-diagonal correlations reinforce our observation of a nonzero mutual information content between the cloud electrons. This implies that the electronic cloud contains, in general, interaction terms beyond the Fermi liquid density-density interaction leading to nonzero entanglement content.

## VII. CONCLUSIONS

The Kondo problem [2] is one of the oldest and most well-studied problems of electronic correlations in condensed matter physics [6,7]. The unitary RG analysis of the Kondo Hamiltonian leads to a zero-temperature phase diagram revealing a strong-coupling fixed point for an antiferromagnetic Kondo coupling. At the IR fixed point, we obtained the effective Hamiltonian, the ground-state wave function, and the energy eigenspectrum. This enabled the computation of various thermodynamic quantities such as the impurity susceptibility, specific heat coefficient, Wilson ratio, Wilson number, and thermal entropy, all of which are found to be in good agreement with those obtained from NRG studies [8]. It is also noteworthy that we were able to capture the entire RG (crossover) flow at finite temperatures from the complete effective Hamiltonian [Eq. (D1)] obtained upon reaching the IR stable fixed point [as seen, for instance, for the susceptibility  $\chi(T)$  in Fig. 13 in Appendix D]. As the URG relies purely on unitary transformations, the eigenspectrum is preserved under the RG flow, and thence so is the partition function. Thus, at each RG fixed point, the effective Hamiltonian equation (D1) enables the construction of the density matrix for a given temperature scale  $k_B T$ , such that one can compute the finite-temperature partition function [Eq. (11)].

Furthermore, we found that the effective Hamiltonian for the Kondo cloud [Eq. (29)], obtained by integrating out the impurity spin, contains a density-density repulsion (corresponding to a Fermi liquid) as well as a four-fermion interaction term. In order to better understand the roles of

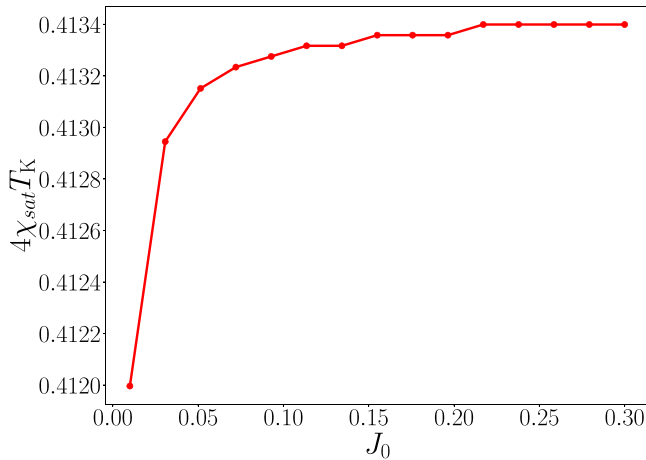


FIG. 13. Variation of the Wilson number  $W = 4T_K\chi_{\text{sat}}$  with bare Kondo coupling  $J_0$ .  $T_K$  corresponds to the Kondo temperature. See discussion in text.

the two types of electronic correlations, we performed a comparative study of the RG evolution of four-point number diagonal and number off-diagonal correlators. By using the singlet IR ground-state wave function obtained from the URG analysis, we also studied the RG evolution of the mutual information (an entanglement-based measure) between (a) the impurity and an electron in the cloud and (b) two electrons in the cloud. The results show strong interelectronic as well as electron-impurity entanglement upon approaching the IR fixed point. This is in agreement with the presence of both types of two-particle correlators at the IR ground state. We find that both the number diagonal and number off-diagonal correlators reach the same value at the IR fixed point, indicating that the electronic configuration within the Kondo cloud is not simply a local Fermi liquid. The large entanglement within the Kondo cloud is an indication of the spin singlet it forms together with the impurity spin. This is an example of quantum mechanics at the macroscale: Impurity-bath correlations drive many-particle entanglement between bath electrons, signaling the emergence of a collective spin that binds with the impurity. Given that the Kondo problem represents a simple model for a single qubit coupled to a fermionic environment, our insights can spur further investigations into more complex qubit-bath interactions relevant to the realization and workings of present-day quantum computers in noisy environments.

The calculation of impurity susceptibility in Appendix D 1 defines the Kondo temperature as that energy scale below which only the singlet state contributes to the susceptibility and the other states in the entangled four-dimensional Hilbert space of the impurity spin and the total conduction electron spin drop out. The subsequent calculation of the

wave-function renormalization  $Z = 1$  in Appendix C backs up the presence of a local Fermi liquid phase at the fixed point. In this way, the low-energy physics of the Kondo model can be captured in great depth purely from the URG fixed-point Hamiltonian. An important point can now be highlighted. The physics of the emergent Kondo cloud Hamiltonian (Sec. V) is found to be in good agreement with that of the local Fermi liquid. This includes various thermodynamic quantities (e.g., the impurity susceptibility, specific heat, thermal entropy, etc.) and the Wilson ratio (see Appendixes D 1 and D 2). We have found that the  $k$ -space Kondo cloud effective Hamiltonian describes an extended real-space object composed of electron waves with extent greater than  $\xi_K$ . On the other hand, the local Fermi liquid is found to reside at a distance  $\xi_K$  from the impurity. Thus it appears tempting to conclude that there exists a holographic bulk-boundary relationship between the Kondo cloud system and the local Fermi liquid. We speculate that the emergent change in the Luttinger volume [see Eq. (C11)] of the conduction bath at the strong-coupling fixed point corresponds to the winding number topological quantity [88] that signals such a holography. We do not know at present whether the effective theory for the Kondo cloud found by us can be related to a bulk gravity theory obtained from an anti-de Sitter and conformal field theory (AdS-CFT) treatment [89]. We leave this for future work.

Future studies need to be performed to investigate the nature of the correlated metal comprising the Kondo cloud. This work also opens up the prospect of performing a similar study on other variants of the Kondo problem, such as the multichannel Kondo model [38–49]. The current method can allow one to investigate the critical properties of the overscreened multichannel Kondo intermediate-coupling fixed point. The low-energy effective Hamiltonian of such models should be helpful in identifying the microscopic origins of the non-Fermi-liquid phase of such a fixed point. Entanglement studies of the zero mode will also be helpful in identifying the breakdown of screening, and such studies will lay bare the distinction between various variants of the Kondo impurity models.

## ACKNOWLEDGMENTS

The authors thank P. Majumdar, A. Mitchell, S. Sen, S. Patra, M. Mahankali, and R. K. Singh for several discussions and feedback. Anirban Mukherjee thanks the CSIR, Government of India, and IISER Kolkata for funding through a research fellowship. Abhirup Mukherjee thanks IISER Kolkata for funding through a research fellowship. Anirban Mukherjee, Abhirup Mukherjee, and S.L. thank JNCASR, Bangalore, for hospitality at the inception of this work. N.S.V. acknowledges funding from JNCASR and a SERB grant (EMR/2017/005398). We thank two anonymous referees for their helpful comments and suggestions.

## APPENDIX A: CALCULATION OF EFFECTIVE HAMILTONIAN FROM URG

Starting from the Kondo Hamiltonian equation (1) and using the URG-based Hamiltonian RG equation (10), we obtain the renormalized Hamiltonian:

$$\begin{aligned} \Delta \hat{H}_{(j)} = & \sum_{\substack{m=1, \\ \beta=\uparrow/\downarrow}}^{n_j} \frac{(J^{(j)})^2 \tau_{j,\hat{s}_m,\beta}}{2(2\omega\tau_{j,\hat{s}_m,\beta} - \epsilon_{j,l}\tau_{j,\hat{s}_m,\beta} - J^{(j)}S^z s_{j,\hat{s}_m}^z)} \times \left[ S^a S^b \sigma_{\alpha\beta}^a \sigma_{\beta\gamma}^b \sum_{\substack{(j_1, j_2 < j), \\ n, o}} c_{j_1, \hat{s}_n, \alpha}^\dagger c_{j_2, \hat{s}_o, \gamma} (1 - \hat{n}_{j, \hat{s}_m, \beta}) \right. \\ & \left. + S^b S^a \sigma_{\beta\gamma}^b \sigma_{\alpha\beta}^a \sum_{\substack{(j_1, j_2 < j), \\ n, o}} c_{j_2, \hat{s}_o, \gamma} c_{j_1, \hat{s}_n, \alpha}^\dagger \hat{n}_{j, \hat{s}_m, \beta} \right] + \sum_{\substack{m=1, \\ \beta=\uparrow/\downarrow}}^{n_j} \frac{(J^{(j)})^2}{2(2\omega\tau_{j,\hat{s}_m,\beta} - \epsilon_{j,l}\tau_{j,\hat{s}_m,\beta} - J^{(j)}S^z s_{j,\hat{s}_m}^z)} \\ & \times \left[ S^x S^y \sigma_{\alpha\beta}^x \sigma_{\beta\alpha}^y c_{j,\hat{s}_m,\alpha}^\dagger c_{j,\hat{s}_m,\beta} c_{j,\hat{s}_m,\beta}^\dagger c_{j,\hat{s}_m,\alpha} + S^y S^x \sigma_{\alpha\beta}^y \sigma_{\beta\alpha}^x c_{j,\hat{s}_m,\beta}^\dagger c_{j,\hat{s}_m,\alpha} c_{j,\hat{s}_m,\alpha}^\dagger c_{j,\hat{s}_m,\beta} \right]. \end{aligned} \quad (\text{A1})$$

The first term in Eq. (A1) corresponds to the renormalization of the Kondo coupling and describes the  $s$ - $d$  exchange interactions for the entangled degrees of freedom

$$\begin{aligned} \Delta H_{(j)}^1 = & \sum_{\substack{m=1, \\ \beta=\uparrow/\downarrow}}^{n_j} \frac{(J^{(j)})^2 \tau_{j,\hat{s}_m,\beta}}{(2\omega\tau_{j,\hat{s}_m,\beta} - \epsilon_{j,l}\tau_{j,\hat{s}_m,\beta} - J^{(j)}S^z s_{j,\hat{s}_m}^z)} \sum_{\substack{(j_1, j_2 < j), \\ n, o}} \mathbf{S} \cdot c_{j_1, \hat{s}_n, \alpha}^\dagger \frac{\sigma_{\alpha\beta}}{2} c_{j_2, \hat{s}_o, \beta} \\ = & \frac{1}{2} \sum_{\substack{m=1, \\ \beta=\uparrow/\downarrow}}^{n_j} \frac{\tau_{j,\hat{s}_m,\beta} (J^{(j)})^2 [(2\omega\tau_{j,\hat{s}_m,\beta} - \epsilon_{j,l}\tau_{j,\hat{s}_m,\beta}) + J^{(j)}S^z s_{j,m}^z]}{(\omega - \frac{\epsilon_{j,l}}{2})^2 - \frac{(J^{(j)})^2}{16}} \sum_{\substack{(j_1, j_2 < j), \\ n, o}} \mathbf{S} \cdot c_{j_1, \hat{s}_n, \alpha}^\dagger \frac{\sigma_{\alpha\beta}}{2} c_{j_2, \hat{s}_o, \beta} \\ = & \frac{1}{2} \left[ \sum_{\substack{m=1, \\ \beta=\uparrow/\downarrow}}^{n_j} \frac{(J^{(j)})^2 [(\frac{\omega}{2} - \frac{\epsilon_{j,l}}{4})]}{(\omega - \frac{\epsilon_{j,l}}{2})^2 - \frac{(J^{(j)})^2}{16}} + \frac{1}{2} \sum_{m=1}^{n_j} \frac{(J^{(j)})^3 S^z s_{j,m}^z (\tau_{j,\hat{s}_m,\uparrow} + \tau_{j,\hat{s}_m,\downarrow})}{(\omega - \frac{\epsilon_{j,l}}{2})^2 - \frac{(J^{(j)})^2}{16}} \right] \sum_{\substack{(j_1, j_2 < j), \\ n, o}} \mathbf{S} \cdot c_{j_1, \hat{s}_n, \alpha}^\dagger \frac{\sigma_{\alpha\beta}}{2} c_{j_2, \hat{s}_o, \beta} \\ = & \frac{n_j (J^{(j)})^2 [(\omega - \frac{\epsilon_{j,l}}{2})]}{(\omega - \frac{\epsilon_{j,l}}{2})^2 - \frac{(J^{(j)})^2}{16}} \mathbf{S} \cdot \sum_{\substack{(j_1, j_2 < j), \\ n, o}} c_{j_1, \hat{s}_n, \alpha}^\dagger \frac{\sigma_{\alpha\gamma}}{2} c_{j_2, \hat{s}_o, \gamma}. \end{aligned} \quad (\text{A2})$$

In the second-to-last step of the calculation, we have used the result  $\tau_{j,\hat{s}_m,\uparrow}^2 = \frac{1}{4}$ , where  $\tau_{j,\hat{s}_m,\uparrow} = \hat{n}_{j,\hat{s}_m,\uparrow} - \frac{1}{2}$ . In obtaining the last step of the calculation we have assumed  $\epsilon_{j,l} = \epsilon_j$  for a circular Fermi surface geometry. Furthermore, we have replaced  $\tau_{j,\hat{s}_m,\uparrow}$  and  $\tau_{j,\hat{s}_m,\downarrow}$  by their eigenvalues,  $\tau_{j,\hat{s}_m,\uparrow} = -\tau_{j,\hat{s}_m,\downarrow} = \frac{1}{2}$ , i.e., the resulting decoupled electronic wave vector  $|j, \hat{s}_m\rangle$  carries a nonzero spin angular momentum. This configuration promotes the spin scattering between the Kondo impurity and the fermionic bath. The second term in Eq. (A1) corresponds to the renormalization of the number diagonal Hamiltonian for the immediately disentangled electronic states  $|j, \hat{s}_m, \sigma\rangle$ :

$$\Delta H_{(j)}^2 = \sum_{\substack{m=1, \\ \beta=\uparrow/\downarrow}}^{n_j} \frac{(J^{(j)})^2}{(2\omega\tau_{j,\hat{s}_m,\beta} - \epsilon_{j,l}\tau_{j,\hat{s}_m,\beta} - J^{(j)}S^z s_{j,\hat{s}_m}^z)} \left[ S^x S^y \sigma_{\alpha\beta}^x \sigma_{\beta\alpha}^y c_{j,\hat{s}_m,\alpha}^\dagger c_{j,\hat{s}_m,\beta} c_{j,\hat{s}_m,\beta}^\dagger c_{j,\hat{s}_m,\alpha} \right. \quad (\text{A3})$$

$$\left. + S^y S^x \sigma_{\alpha\beta}^y \sigma_{\beta\alpha}^x c_{j,\hat{s}_m,\beta}^\dagger c_{j,\hat{s}_m,\alpha} c_{j,\hat{s}_m,\alpha}^\dagger c_{j,\hat{s}_m,\beta} \right] \quad (\text{A4})$$

$$= \sum_{\substack{m=1, \\ \beta=\uparrow/\downarrow}}^{n_j} \frac{(J^{(j)})^2}{(2\omega\tau_{j,\hat{s}_m,\beta} - \epsilon_{j,l}\tau_{j,\hat{s}_m,\beta} - J^{(j)}S^z s_{j,\hat{s}_m}^z)} S^z \frac{\sigma_{\alpha\alpha}^z}{2} \left[ \hat{n}_{j,\hat{s}_m,\alpha} (1 - \hat{n}_{j,\hat{s}_m,\beta}) - \hat{n}_{j,\hat{s}_m,\beta} (1 - \hat{n}_{j,\hat{s}_m,\alpha}) \right] \quad (\text{A5})$$

$$= \sum_{m=1}^{n_j} \frac{(J^{(j)})^2}{(2\omega\tau_{j,\hat{s}_m,\beta} - \epsilon_{j,l}\tau_{j,\hat{s}_m,\beta} - J^{(j)}S^z s_{j,\hat{s}_m}^z)} S^z s_{j,\hat{s}_m}^z, \quad (\text{A6})$$

where we have used  $\hat{n}_{j,\hat{s}_m,\alpha} (1 - \hat{n}_{j,\hat{s}_m,\beta}) - \hat{n}_{j,\hat{s}_m,\beta} (1 - \hat{n}_{j,\hat{s}_m,\alpha}) = \hat{n}_{j,\hat{s}_m,\alpha} - \hat{n}_{j,\hat{s}_m,\beta}$  in the last step, and the spin density for the state  $|j, \hat{s}_m\rangle$  is given by  $s_{j,\hat{s}_m}^z = \frac{1}{2}(\hat{n}_{j,\hat{s}_m,\uparrow} - \hat{n}_{j,\hat{s}_m,\downarrow})$ . In obtaining the above RG equation we have replaced  $\hat{\omega}_{(j)} = 2\omega\tau_{j,\hat{s}_m,\beta}$ . We set the electronic configuration  $\tau_{j,\hat{s}_m,\uparrow} = -\tau_{j,\hat{s}_m,\downarrow} = \frac{1}{2}$  to account for the spin scattering between the Kondo impurity and the fermionic bath. The operator  $\hat{\omega}_{(j)}$  [Eq. (7)] for RG step  $j$  is determined by the occupation number diagonal piece of the Hamiltonian  $H_{(j-1)}^D$  attained at the next RG step  $j-1$ . This demands a self-consistent treatment of the RG equation to determine the  $\omega$ . In this fashion, two-particle and higher-order quantum fluctuations are automatically encoded into the RG dynamics of  $\hat{\omega}$ . In this paper, however, we restrict our study by ignoring the RG contribution in  $\omega$ . The electron and hole configurations ( $|1_{j,\hat{s}_m,\beta}\rangle$  and  $|0_{j,\hat{s}_m,\beta}\rangle$ )

respectively) of the disentangled electronic state (and associated with energy  $\pm\epsilon_{j,l}$ ) is accounted for by the fluctuation energy scales  $\pm\omega$ . From the above Hamiltonian RG equation (A2), we can obtain the form of the Kondo coupling RG equation (13)

$$\Delta J^{(j)} = \frac{n_j(J^{(j)})^2 \left[ \omega - \frac{\epsilon_{j,l}}{2} \right]}{\left( \frac{\epsilon_{j,l}}{2} - \omega \right)^2 - \frac{(J^{(j)})^2}{16}}. \quad (\text{A7})$$

It is easy to generalize this method to the more general anisotropic Kondo model with distinct transverse ( $J_\perp$ ) and Ising ( $J_z$ ) couplings:

$$J_z S^z \sum_{kk'} \frac{1}{2} (c_{k\uparrow}^\dagger c_{k'\uparrow} - c_{k\downarrow}^\dagger c_{k'\downarrow}) + \frac{1}{2} J_\perp S^+ \sum_{kk'} c_{k\downarrow}^\dagger c_{k'\uparrow} + \frac{1}{2} J_\perp S^- \sum_{kk'} c_{k\uparrow}^\dagger c_{k'\downarrow}. \quad (\text{A8})$$

We now briefly sketch the calculation.

(i) Since the denominator involves the diagonal  $S^z S^z$  part of the Hamiltonian, only the Ising coupling  $J_z$  will enter the denominator of the RG equation.

(ii) The Ising coupling  $J_z$  will be renormalized only by scattering processes that involve one  $S^+$  operator and one  $S^-$  operator, so that the corresponding scattering vertices that renormalize  $J_z$  are of strength  $J_\perp^2$ .

(iii) On the other hand, the transverse coupling  $J_\perp$  will be renormalized only by processes that involve one  $S^\pm$  operator and one  $S^z$  operator, so that the corresponding vertices are of strength  $J_z J_\perp$ .

With these modifications, the final result of Eq. (A2) becomes

$$\frac{n_j(\omega - \frac{\epsilon_j}{2})}{\left(\omega - \frac{\epsilon_{j,l}}{2}\right)^2 - \frac{(J_z^{(j)})^2}{16}} \left[ (J_\perp^{(j)})^2 \sum_{\substack{(j_1, j_2 < j), \\ n, o, \alpha}} S^z \sigma_{\alpha\alpha}^z c_{j_1, \delta_n, \alpha}^\dagger c_{j_2, \delta_o, \alpha} + J_z^{(j)} J_\perp^{(j)} \left( \sum_{\substack{(j_1, j_2 < j), \\ n}} S^+ c_{j_1, \delta_n, \downarrow}^\dagger c_{j_2, \delta_o, \uparrow} + \text{H.c.} \right) \right]. \quad (\text{A9})$$

The RG equations for the Ising and transverse couplings can now be read off from the renormalized Hamiltonian:

$$\begin{aligned} \Delta J_z^{(j)} &= \frac{n_j (J_\perp^{(j)})^2 \left[ \omega - \frac{\epsilon_{j,l}}{2} \right]}{\left( \omega - \frac{\epsilon_{j,l}}{2} \right)^2 - \frac{(J_z^{(j)})^2}{16}}, \\ \Delta J_\perp^{(j)} &= \frac{n_j J_z^{(j)} J_\perp^{(j)} \left[ \omega - \frac{\epsilon_{j,l}}{2} \right]}{\left( \omega - \frac{\epsilon_{j,l}}{2} \right)^2 - \frac{(J_z^{(j)})^2}{16}}. \end{aligned} \quad (\text{A10})$$

These coupled RG equations have the same RG invariant as the Berezinskii-Kosterlitz-Thouless (BKT) RG equations [90,91] as well as the 1D Hubbard model RG equations [63]:

$$\frac{\Delta J_z^{(j)}}{\Delta J_\perp^{(j)}} = \frac{J_\perp^{(j)}}{J_z^{(j)}} \Rightarrow J_\perp^{(j)2} - J_z^{(j)2} = \text{const.} \quad (\text{A11})$$

One can also show that the anisotropy in the couplings is irrelevant by writing the RG equation for the anisotropy parameter  $\kappa = J_\perp^{(j)} - J_z^{(j)}$ .

$$\Delta \kappa = \frac{n_j J_t^{(j)} (J_\perp^{(j)} - J_z^{(j)}) \left[ \omega - \frac{\epsilon_{j,l}}{2} \right]}{\left( \omega - \frac{\epsilon_{j,l}}{2} \right)^2 - \frac{(J_z^{(j)})^2}{16}}. \quad (\text{A12})$$

Dividing this equation by the RG equation of  $J_z^{(j)}$  gives

$$\frac{\Delta \kappa}{\Delta J_z^{(j)}} = -\frac{\kappa}{J_\perp^{(j)}}. \quad (\text{A13})$$

Since both  $\Delta J_z^{(j)}$  and  $J_\perp^{(j)}$  are positive in the strong-coupling regime, we find that  $\Delta \kappa / \kappa < 0$ . This relation implies that if  $\kappa$  is initially positive (negative), the renormalization is negative (positive), and  $\kappa$  flow towards zero. This shows that all strong-coupling flows enforce the irrelevance of the anisotropy parameter  $\kappa$ .

## APPENDIX B: EFFECTIVE HAMILTONIAN FOR THE LOCAL FERMI LIQUID

The central resonance in the impurity spectral function can be attributed to quasiparticle excitations arising from the local Fermi liquid component of the effective

Hamiltonian. Here, we will derive an effective Hamiltonian for low-energy excitations in the singlet subspace of the fixed-point theory and hence expose the local Fermi liquid component.

To consider the local states as ground states, we will drop the kinetic energy part and start with the following zeroth

Hamiltonian:

$$\mathcal{H}_{\text{loc}}^* = \underbrace{J^* \vec{S}_d \cdot \vec{s}}_{H_0} - t^* \underbrace{\sum_{\sigma, (0,l)} c_{0\sigma}^\dagger c_{l,\sigma}}_V + \text{H.c.} \quad (\text{B1})$$

The four ground states of  $H_0$  are

$$|\phi_i^{(0)}\rangle = \underbrace{|\chi_i\rangle}_{\text{site 1}} \otimes \frac{1}{\sqrt{2}}(|\uparrow, \downarrow\rangle - |\downarrow, \uparrow\rangle), \quad i \in [1, 4],$$

$$\{\chi_i\} = \{0, \uparrow, \downarrow, 2\}, \quad E = -\frac{3J^*}{4}. \quad (\text{B2})$$

In the singlet part, the first entry is the configuration of the zeroth site, while the second entry is the configuration of the impurity site.

Since  $V$  and  $V^3$  take  $|\phi_{2,4}^{(0)}\rangle$  to a completely orthogonal subspace, the first- and third-order corrections are 0. The second-order shift in the ground-state energy for a state  $\phi^{(0)}$  is given by

$$E^{(2)} = \sum_{i \neq \phi^{(0)}} \frac{|\langle \phi^{(0)} | V | i \rangle|^2}{E_\phi^{(0)} - E_i}. \quad (\text{B3})$$

This second-order shift for both the up-spin and double-occupied states [and hence the down and empty states, using SU(2) and particle-hole (p-h) symmetries] comes out to be

$$E^{(2)} = -\frac{4t^2}{3J^*}, \quad (\text{B4})$$

so that the effective Hamiltonian at second order is simply a constant. We move on to the fourth-order correction. The general formula is quite formidable, so we only write down the terms that are not outright zero for this problem:

$$E^{(4)} = \sum_{\substack{i^{(0)} \neq \phi, \\ j^{(0)} \neq \phi, \\ k^{(0)} \neq \phi}} \frac{V_{\phi,k} V_{k,j} V_{j,i} V_{i,\phi}}{E_{\phi,k} E_{\phi,j} E_{\phi,i}} - E_\phi^{(2)} \sum_{m^{(0)} \neq \phi} \frac{|V_{m,\phi}|^2}{(E_{\phi,m})^2}, \quad (\text{B5})$$

where  $V_{x,y} = \langle x^{(0)} | V | y^{(0)} \rangle$  and  $E_{x,y} = E_x^{(0)} - E_y^{(0)}$ . At fourth order,  $|\phi_2^{(0)}\rangle$  is first excited to  $|0, 2, \uparrow\rangle$  or  $|2, 0, \uparrow\rangle$  and then to the spin-triplet subspace. The total effective Hamiltonian up to fourth order (and up to a constant energy shift) is

$$H_{\text{loc}}^{\text{eff}} = -4\alpha \frac{t^4}{J^{*3}} \sum_{\sigma} \hat{n}_{1\sigma} + 8\alpha \frac{t^4}{J^{*3}} \hat{n}_{1\uparrow} \hat{n}_{1\downarrow}. \quad (\text{B6})$$

The presence of the repulsive correlation term means that electrons that want to occupy the first site will face a repulsion from an electron already present there and the effective Hamiltonian behaves like a local Fermi liquid [13] on the first site.

### APPENDIX C: SCATTERING PHASE SHIFT OF CONDUCTION ELECTRONS AT STRONG COUPLING AND WAVE-FUNCTION RENORMALIZATION

In general, the conduction electrons will suffer a phase shift as they scatter off the impurity. We will obtain an explicit form for this phase shift in terms of the fixed-point coupling  $J^*$ , by writing down a simple Hamiltonian that models the low-energy theory. We will drop the states of the triplet subspace

and retain only the singlet state and the double and hole states of the zeroth site. In order to avoid any two-particle terms, we will drop the impurity site because it is already frozen in the singlet. Also, since the double and hole states are at zero energy, they will drop out of the Hamiltonian, and we will model the zeroth site in the form of a single spin. We define  $|0_\sigma\rangle$  as the state where the zeroth site has a single electron of spin  $\sigma$  and  $|0_0\rangle$  and  $|0_2\rangle$  as the states with zero and two electrons on the zeroth site, respectively. Then,

$$\text{spectrum of zeroth site} \rightarrow \begin{cases} \text{state} & \text{energy} \\ |0_\sigma\rangle & -\frac{3J^*}{4} \\ |0_0\rangle, |0_2\rangle & 0. \end{cases} \quad (\text{C1})$$

The total simplified Hamiltonian can therefore be written completely in terms of the single-particle states  $|0_\sigma\rangle$  and  $|k_\sigma\rangle$ .  $|k_\sigma\rangle$  is the conduction electron state of momentum  $k$  and spin  $\sigma$ . This Hamiltonian preserves the spin of the zeroth site and the conduction electrons separately, and the Hamiltonian for a particular spin is

$$\mathcal{H}_\sigma = \epsilon_0 |0_\sigma\rangle \langle 0_\sigma| + \sum_k [-t(|0_\sigma\rangle \langle k_\sigma| + \text{H.c.}) + \epsilon_k |k_\sigma\rangle \langle k_\sigma|], \quad (\text{C2})$$

where  $\epsilon_0 = -\frac{3J^*}{4}$  is the effective on-site energy of the zeroth site. The matrix elements of the retarded single-particle Green's function for spin  $\sigma$ ,  $G^\sigma$ , satisfy the equation  $\sum_\beta (\omega - \mathcal{H}_\sigma)_{\alpha\beta} G_{\beta\gamma} = \delta_{\alpha\gamma}$ , where  $\alpha$ ,  $\beta$ , and  $\gamma$  represent matrix elements between any pair of states among  $0_\sigma$  and  $\{k_\sigma\}$  and  $\delta$  is the Kronecker delta [92]. Solving the equations for  $G_{00}^\sigma$  gives

$$G_{00}^\sigma(\omega) = \frac{1}{\omega - \epsilon_0 - \Sigma(\omega)}. \quad (\text{C3})$$

$\Sigma(\omega) = \sum_k \frac{t^2}{\omega - \epsilon_k} = \int d\epsilon \frac{t^2 \rho(\epsilon)}{\omega - \epsilon}$  is the self-energy of the zeroth site of the bath because of hybridization with the rest of the bath through the hopping term  $t$ . The imaginary part is given by  $\text{Im} \Sigma_I(\omega) = -\pi \rho(\omega) t^2$ . Since  $\epsilon_0 \gg t^2$ , we can drop the real part of the self-energy in the denominator. The  $T$  matrix of the conduction electrons can now be calculated using this impurity Green's function [93]:

$$T_{kk'}^\sigma(\omega) = t^2 G_{00}^\sigma(\omega) = t^2 \frac{\omega - \epsilon_0 + i \text{Im} \Sigma_I}{(\omega - \epsilon_0)^2 + \text{Im} \Sigma_I^2}. \quad (\text{C4})$$

From scattering theory, it can be shown that the phase shift  $\delta_{k\sigma}^{\text{FL}}$  of the conduction electron state  $|k\sigma\rangle$  is given by the phase of  $T_{kk}$  [94]:

$$\tan \delta_{k\sigma}^{\text{FL}}(\omega) = \frac{\text{Im} \Sigma_I}{\omega - \epsilon_0} = \frac{-\pi \rho(\omega) t^2}{\omega + \frac{3J^*}{4}}. \quad (\text{C5})$$

Note that there is an additional phase shift that we have not accounted for; when we removed the zeroth site from the lattice, all the wave functions got shifted by a distance of  $a$ :  $\psi_k(x) \sim \sin(kx) \rightarrow \sin(kx - ka)$ . This is equivalent to a phase shift of  $\delta_{k\sigma}^0 = ka$ . The total phase shift is therefore

$$\delta_{k\sigma}^{\text{tot}}(\omega) \equiv \delta_{k\sigma}^0 + \delta_{k\sigma}^{\text{FL}}(\omega) = ka + \tan^{-1} \frac{-\pi \rho(\omega) t^2}{\omega + \frac{3J^*}{4}}. \quad (\text{C6})$$

Furthermore, following the arguments involving the Friedel sum rule given in Ref. [95], we know that the total scattering

phase shift in the ground state of the single-impurity Anderson model (SIAM) at the Fermi surface is equal to  $\pi$  times the impurity occupation  $n_d$ . The Kondo model corresponds to the local-moment regime of the SIAM and possesses a value of  $n_d = 1$ . It then follows that

$$\delta_{k_F}^{\text{tot}}(0) = \pi \times n_d = \pi. \quad (\text{C7})$$

Furthermore, we know that since  $k_{F\sigma} = 1/2a$  for a half-filled one-dimensional Fermi volume (for an  $s$ -wave Kondo exchange coupling), the phase shift  $\delta_{k_F}^0$  is given by

$$\delta_{k_F}^0 = \sum_{\sigma} \delta_{k_F\sigma}^0 = \sum_{\sigma} k_{F\sigma} a = \pi = \delta_{k_F}^{\text{tot}}(0). \quad (\text{C8})$$

Substituting  $\delta_{k_F}^0 = \delta_{k_F}^{\text{tot}}(0)$  into Eq. (C6) then indicates that the scattering phase shift for the Landau quasiparticle  $\delta^{\text{FL}}$  vanishes identically at the Fermi surface, and the total phase shift is determined purely by  $\delta_{k_F}^0$ .

The phase shift can also be connected to the overlap integral between the ground states  $|\Psi_0\rangle$  and  $|\Psi\rangle$  before and after adding the local interaction, respectively. The local interaction can take the form of either the Kondo coupling between the impurity and the Kondo cloud, or a hopping between the zeroth site and the rest of the conduction bath. In the former case, the ground-state  $|\Psi_0\rangle$  is that of a decoupled conduction bath, and  $|\Psi\rangle$  corresponds to the ground state of the conduction electrons in the presence of a strong Kondo coupling. In the latter case,  $|\Psi_0\rangle$  is the ground state of a conduction bath from which the zeroth site (i.e., the site strongly coupled with the impurity) is removed, and  $|\Psi\rangle$  is that of the same system but with a small hopping between the zeroth and first sites of the conduction gas.

Following Anderson's orthogonality theorem [96], its extension by Yamada and Yosida [97], and the generalized Friedel sum rule due to Langer and Ambegaokar [98], the square of the overlap integral (often called the wave-function renormalization) is given by

$$Z \equiv |\langle \Psi | \Psi_0 \rangle|^2 = N^{-\frac{1}{\pi^2} \delta_{k_F}^0(0)^2}, \quad (\text{C9})$$

where  $N$  is the total number of conduction electrons and  $\delta_{k_F}^0(0)$  is the phase shift produced by the local perturbation at the Fermi surface. In the thermodynamic limit, this expression simplifies to

$$Z(N \rightarrow \infty) = 1 \quad \text{if } \delta_{k_F}^0(0) = 0, \text{ and } 0 \text{ otherwise.} \quad (\text{C10})$$

For the first case of the local interaction mentioned above (i.e., for the Kondo coupling), we obtain the wave-function overlap ( $Z_{\text{imp}}$ ) in terms of the total phase shift:  $Z_{\text{imp}} = N^{-\frac{1}{\pi^2} (\delta_{k_F}^{\text{tot}}(0))^2} \rightarrow 0$  in the limit  $N \rightarrow \infty$ . This shows the *orthogonality catastrophe* between the ground states of the conduction bath in the local-moment and strong-coupling phases. Furthermore, following Ref. [99], the orthogonality catastrophe reflects a change in the Luttinger volume ( $\Delta N_L$ ) of the conduction bath:

$$\Delta N_L = \frac{\delta_{k_F}^0(0)}{\pi} = 1. \quad (\text{C11})$$

This increase in the number of electrons inside the Fermi volume is nothing but the ‘‘large Fermi surface’’ effect seen

in heavy fermionic systems [100–103]. Here, the effect is infinitesimal because of the local nature of the impurity.

In the second case (i.e., with the zeroth site as the local perturbation), the relevant phase shift is  $\delta_{k_F}^{\text{FL}}(0) = 0$ , and the overlap integral then pertains to the quasiparticle residue of the local Fermi liquid:  $Z_{\text{FL}} = N^{-\frac{1}{\pi^2} (\delta_{k_F}^{\text{FL}}(0))^2} = 1$ . Furthermore, from Ref. [94], the Wilson ratio  $R$  of the local Fermi liquid is given by

$$R = 1 + \sin^2 \left( \frac{\delta_{k_F}^0(0)}{2} \right) = 1 + \sin^2 \left( \frac{\pi}{2} \right) = 2. \quad (\text{C12})$$

## APPENDIX D: CALCULATION OF THERMODYNAMIC QUANTITIES

### 1. Impurity contribution to the magnetic susceptibility

The complete effective Hamiltonian for the impurity spin  $\mathbf{S}$ , the Kondo cloud spin  $\mathbf{s}$ , and the electrons that comprise the local Fermi liquid has the form

$$H_2 = \epsilon_* \sum_{m,\sigma} \hat{n}_{*,m,\sigma} + J^* \mathbf{S} \cdot \mathbf{s} + J^* S^z \sum_m s_{*,m}^z. \quad (\text{D1})$$

The Hamiltonian  $H_2$  has several conserved quantities, which we depict below:

$$[H_2, S^z + s^z] = 0, \quad [H_2, s_{*,m}^z] = 0 \quad \forall 1 \leq m \leq n_j, \quad (\text{D2})$$

such that  $[H^*, S_{\text{tot}}^z] = 0$ , where  $S_{\text{tot}}^z = S^z + s^z + \sum_m s_{*,m}^z$ . Therefore the eigenvalues of  $|s_{*,m}^z = \uparrow / \downarrow\rangle$  are good quantum numbers; this is simply an outcome of the URG method. For the purposes of computing the impurity magnetization and susceptibility, we keep only the effective impurity–Kondo-electron-cloud Hamiltonian from  $H_2$  above:

$$H_K^* = J^* \mathbf{S} \cdot \mathbf{s} + B S^z, \quad (\text{D3})$$

where we have introduced a local magnetic field  $B$  that couples to the impurity magnetic moment through a Zeeman coupling.

We can now obtain the impurity magnetization and susceptibility from the effective Hamiltonian  $H_K^*$ . The four-state eigenspectrum of  $H_K^*$  is given by

$$E_{1,2} = \frac{1}{2} \left( -\frac{J^*}{2} \pm \sqrt{B^2 + J^{*2}} \right), \quad E_{3,4} = \frac{1}{4} J^* - \frac{1}{2} B. \quad (\text{D4})$$

The partition function for this Hamiltonian (with  $\beta = \frac{1}{k_B T}$ ) is given by

$$Z(B) = 2e^{-\beta \frac{J^*}{4}} \cosh \left( \beta \frac{B}{2} \right) + 2e^{\beta \frac{J^*}{4}} \cosh \left( \frac{\beta}{2} (\sqrt{B^2 + J^{*2}}) \right). \quad (\text{D5})$$

The susceptibility is then given by

$$\chi = \lim_{B \rightarrow 0} \frac{d}{dB} \left( \frac{k_B T}{Z(B)} \frac{dZ(B)}{dB} \right) = \frac{\frac{\beta}{4} + \frac{1}{2J^*} e^{\beta \frac{J^*}{2}} \sinh \left( \frac{\beta}{2} J^* \right)}{1 + e^{\beta \frac{J^*}{2}} \cosh \left( \frac{\beta}{2} J^* \right)}. \quad (\text{D6})$$

In the plot of  $4\chi T_K$  (Fig. 12), the red and blue curves represent the contributions to the total susceptibility coming from the  $S^z = 0$  and  $S^z \neq 0$  sectors, respectively. The black curve is the total susceptibility itself. The inset shows a further resolution of the  $S^z = 0$  sector into the  $S = 0$  and

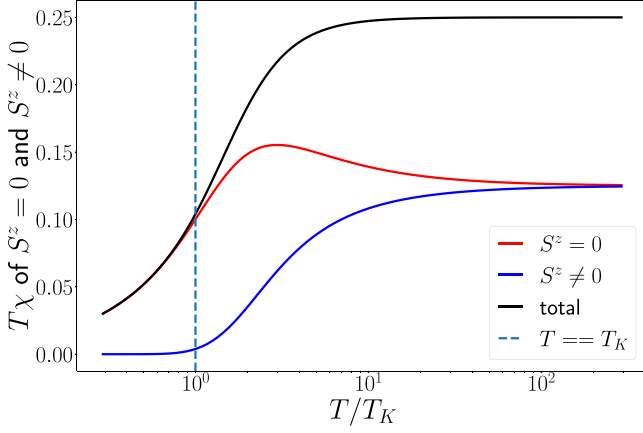


FIG. 14. Variation of  $T\chi$  with  $T/T_K$ .  $T_K$  corresponds to the Kondo temperature. See discussion in text.

$S = 1$  contributions. We can now make several important observations based on Eq. (D6) and the plot. Firstly, at low temperatures  $T \ll T_K$ , almost the entirety of the contribution comes from the singlet state. Near  $T_K$ , the singlet contribution starts dropping, while the  $S^z \neq 0$  contributions start to pick up. In this way, the Kondo temperature scale  $T_K$  arises out of the interplay between symmetry-preserved and symmetry-broken sectors. Coming down from high temperatures,  $T_K$  can be thought of as that temperature beyond which the susceptibility contribution from the symmetry-broken states vanishes.

Secondly, the saturation value of  $4T_K\chi$  as  $\beta \rightarrow \infty$  (i.e.,  $T \rightarrow 0$ ) is given by

$$\chi_{\text{sat}} = \chi(T = 0) = \frac{1}{2J^*}. \quad (\text{D7})$$

We find that the Wilson number  $W = 4T_K\chi_{\text{sat}}$  takes the form  $\frac{2T_K}{J^*}$ . For values of  $J^* \simeq 16.612t$  and  $T_K \simeq 3.433t$  we obtain  $W = 0.413$ . This is in good agreement with the value for  $W$  obtained from NRG [8] and the Bethe ansatz solution of the Kondo problem [9,10]. This is shown in Fig. 12. Furthermore, we show the variation of  $W$  with the bare Kondo coupling  $J$  in Fig. 13. The figure clearly shows the saturation of  $W$  to the

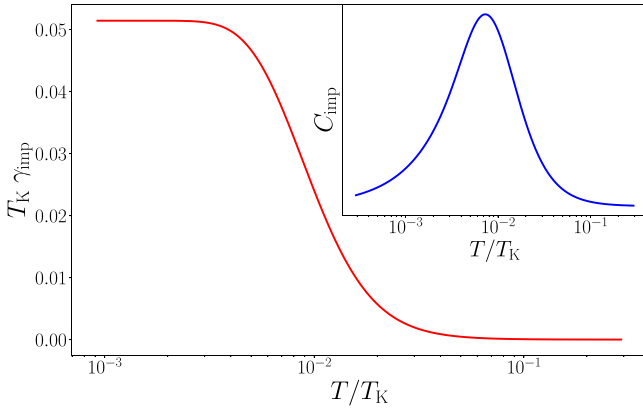


FIG. 15. Variation of  $\gamma_{\text{imp}}T_K$  with  $T/T_K$ .  $T_K$  corresponds to the Kondo temperature. The saturation at low temperatures shows the Fermi-liquid-like behavior. The inset shows the impurity specific heat  $C_{\text{imp}}$ .

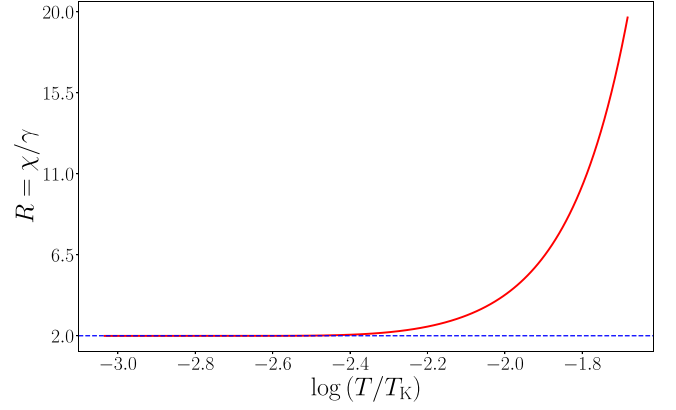


FIG. 16. Variation of the Wilson ratio  $R$  with  $T/T_K$ .  $R$  saturates to a value of 2.009 as  $T \rightarrow 0$ .  $T_K$  corresponds to the Kondo temperature.

value mentioned above as  $J$  flows to the strong-coupling fixed point.

Thirdly, the  $4T_K\chi$ -vs-temperature curve shown in Fig. 12 has a nonmonotonic behavior, i.e., we find a maximum obtained from the transcendental equation  $\frac{d\chi}{d\beta} = 0$ . We confirm from our numerical studies that the temperature corresponding to the maximum value of  $T_K\chi$  tends to  $T_K$  as  $J$  flows to strong coupling. Furthermore, we find that the maximum value of  $T_K\chi$  does not vary with the bare  $J$  in the range  $O(10^{-5}) < J < O(1)$ . As discussed before, this maximum emerges as we go to lower temperatures and indicates that temperature at which the contributions from the  $|\uparrow, \uparrow\rangle$  and  $|\downarrow, \downarrow\rangle$  drop out. Thus the nonmonotonic behavior in  $\chi$  can be directly attributed to the corresponding nonmonotonic behavior in the contribution coming from these states. We note that the impurity susceptibility obtained from NRG treatments of the Kondo problem appears to resemble that obtained by us for the  $S_z = 0$  sector (red curve in Fig. 12) rather than the total susceptibility. We do not presently understand the reason for this discrepancy. However, it is also interesting to note that a similar nonmonotonic behavior of the impurity susceptibility is obtained from a Schwinger boson large- $N$  mean-field approach to the fully screened Kondo model [104].

Finally, we find that the saturation value of  $T \times \chi$  for  $\beta \rightarrow 0$  is given by the universal value  $k_B T\chi(T = \infty) = \frac{1}{4}$ , as shown in Fig. 14. The saturation value at high  $T$  arises from the twofold degenerate impurity and reflects the physics of the (almost isolated) local impurity spin moment, while the vanishing value of  $T\chi$  originates from the formation of the singlet between the Kondo cloud and the impurity spin [second term in Eq. (D1)].

## 2. Impurity contribution to specific heat and thermal entropy

In order to study the thermodynamic properties of the Fermi liquid, we restrict our attention to the density-density terms only. From the density terms we obtain the low-excitation-energy functional accounting for the quasiparticle interaction

$$E = E_0 + \sum_{\mathbf{k}\Lambda\bar{\Lambda}, \Lambda < \Lambda^*} \epsilon_{\mathbf{k}} \delta n_{\mathbf{k}\sigma} + \sum_{\mathbf{k}, \mathbf{k}'} \frac{\epsilon_{\mathbf{k}} \epsilon_{\mathbf{k}'}}{J^*} \delta n_{\mathbf{k}\sigma} \delta n_{\mathbf{k}'\sigma'}. \quad (\text{D8})$$

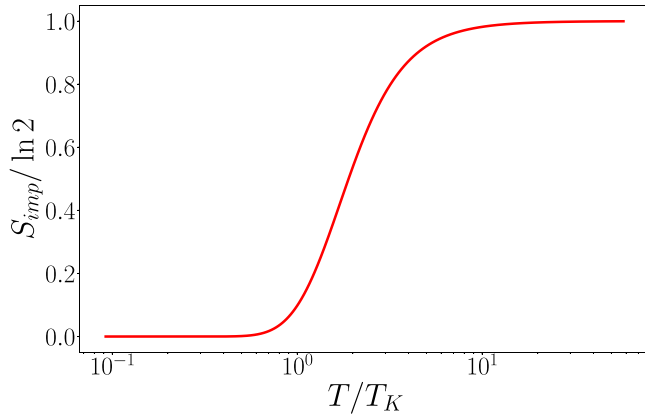


FIG. 17. Impurity contribution to thermal entropy in units of  $\ln 2$ .  $T_K$  corresponds to the Kondo temperature. The high-temperature value of  $\ln 2$  is indicative of a doubly degenerate local moment, while the zero-temperature value of 0 shows that the ground state is a nondegenerate singlet.

This leads to the renormalized one-particle dispersion, where the self-energy term has the following form:

$$\bar{\epsilon}_\Lambda = \epsilon_\Lambda + \Sigma_\Lambda, \quad \Sigma_\Lambda = \left( \sum_{\Lambda', \delta, \sigma'} \frac{\epsilon_\Lambda \epsilon_{\Lambda'}}{J^*} \delta n_{\Lambda', \delta, \sigma'} \right) \quad \text{for } \Lambda < \Lambda^*. \quad (\text{D9})$$

Note that as  $\Lambda \rightarrow 0$ ,  $\Sigma_\Lambda \rightarrow 0$ . Next, we compute the specific heat  $C_{\text{imp}} [\equiv C(J^*) - C(0)]$  of the impurity from the Fermi

distribution of the renormalized quasiparticles

$$C_{\text{imp}} = \sum_{\Lambda, \delta, \sigma} \frac{1}{T^2} \left[ \frac{(\bar{\epsilon}_\Lambda)^2 e^{\beta \bar{\epsilon}_\Lambda}}{(e^{\beta \bar{\epsilon}_\Lambda} + 1)^2} - \frac{(\epsilon_\Lambda)^2 e^{\beta \epsilon_\Lambda}}{(e^{\beta \epsilon_\Lambda} + 1)^2} \right], \quad (\text{D10})$$

where  $C(J^*)$  is the specific heat for the electronic system with the Kondo impurity and  $C(0)$  is the specific heat for the free electronic system without coupling to the Kondo impurity. The specific heat coefficient is given by  $\gamma_{\text{imp}} = \frac{C_{\text{imp}}}{k_B T}$ .

We computed the impurity specific heat using the same set of parameters as used in the computation of the susceptibility and plotted  $\gamma_{\text{imp}} T_K$  in Fig. 15. It is seen that  $\gamma_{\text{imp}} T_K$  rises from 0 at high temperatures  $T > 10^2 T_K$  and saturates at a value  $\gamma_{\text{imp}}(0) = \frac{1}{4J^*}$  for  $T < 10^{-2} T_K$ . The Wilson ratio  $R$  is defined as the ratio of the susceptibility  $\chi_{\text{imp}}$  and the specific heat coefficient  $\gamma_{\text{imp}}$ . It is found that  $R$  saturates to a value  $R = \chi/\gamma_{\text{imp}} = 2.009$  for  $T \ll T_K$  (Fig. 16). We also calculated the impurity thermal entropy from the zero-mode Hamiltonian using the expression

$$S_{\text{imp}}(T) = -\frac{1}{2} \frac{\partial F}{\partial T} = \frac{1}{2} \left[ \ln Z + \frac{\beta}{Z} \sum_i \epsilon_i e^{-\beta \epsilon_i} \right]. \quad (\text{D11})$$

$Z$  and  $\epsilon_i$  are the partition function and energy eigenvalues of the zero-mode Hamiltonian, and the factor of 1/2 comes from the fact that since the impurity and the conduction bath site are symmetrical in the zero-mode Hamiltonian, the impurity contribution to the entropy will be half of the total contribution. This is shown in Fig. 17. At high temperatures, the impurity behaves like a doubly degenerate free spin, contributing an entropy of  $\ln 2$ . At lower temperatures, the impurity is screened within the unique singlet ground state, leading to a vanishing residual entropy.

- 
- [1] J. Schrieffer and P. A. Wolff, *Phys. Rev.* **149**, 491 (1966).  
[2] J. Kondo, *Prog. Theor. Phys.* **32**, 37 (1964).  
[3] Y.-h. Zhang, S. Kahle, T. Herden, C. Stroh, M. Mayor, U. Schlickum, M. Ternes, P. Wahl, and K. Kern, *Nat. Commun.* **4**, 2110 (2013).  
[4] P. W. Anderson and G. Yuval, *Phys. Rev. Lett.* **23**, 89 (1969).  
[5] P. W. Anderson, G. Yuval, and D. Hamann, *Phys. Rev. B* **1**, 4464 (1970).  
[6] P. Anderson, *J. Phys. C: Solid State Phys.* **3**, 2436 (1970).  
[7] K. G. Wilson, *Rev. Mod. Phys.* **47**, 773 (1975).  
[8] R. Bulla, T. A. Costi, and T. Pruschke, *Rev. Mod. Phys.* **80**, 395 (2008).  
[9] N. Andrei, K. Furuya, and J. H. Lowenstein, *Rev. Mod. Phys.* **55**, 331 (1983).  
[10] A. M. Tsvelick and P. B. Wiegmann, *Adv. Phys.* **32**, 453 (1983).  
[11] I. Affleck, *Acta Phys. Pol. B* **26**, 1869 (1995).  
[12] I. Affleck and A. W. W. Ludwig, *Phys. Rev. B* **48**, 7297 (1993).  
[13] P. Nozières, *J. Low Temp. Phys.* **17**, 31 (1974).  
[14] M. Nozaki, S. Ryu, and T. Takayanagi, *J. High Energy Phys.* **10** (2012) 193.  
[15] H. R. Krishnamurthy, C. Jayaprakash, S. Sarker, and W. Wenzel, *Phys. Rev. Lett.* **64**, 950 (1990).  
[16] M. Hanl and A. Weichselbaum, *Phys. Rev. B* **89**, 075130 (2014).  
[17] T. Arai, *J. Appl. Phys. (Melville, NY)* **57**, 3161 (1985).  
[18] M. Gaass, A. K. Hüttel, K. Kang, I. Weymann, J. von Delft, and C. Strunk, *Phys. Rev. Lett.* **107**, 176808 (2011).  
[19] E. S. Sørensen and I. Affleck, *Phys. Rev. B* **53**, 9153 (1996).  
[20] I. Affleck and P. Simon, *Phys. Rev. Lett.* **86**, 2854 (2001).  
[21] P. Simon and I. Affleck, *Phys. Rev. B* **68**, 115304 (2003).  
[22] C. A. Busser, G. B. Martins, L. C. Ribeiro, E. Vernek, E. V. Anda, and E. Dagotto, *Phys. Rev. B* **81**, 045111 (2010).  
[23] L. C. Ribeiro, G. B. Martins, G. Gomez-Silva, and E. V. Anda, *Phys. Rev. B* **99**, 085139 (2019).  
[24] D. Goldhaber-Gordon, H. Shtrikman, D. Mahalu, D. Abusch-Magder, U. Meirav, and M. A. Kastner, *Nature (London)* **391**, 156 (1998).  
[25] S. M. Cronenwett, T. H. Oosterkamp, and L. P. Kouwenhoven, *Science* **281**, 540 (1998).  
[26] J. Schmid, J. Weis, K. Eberl, and K. v. Klitzing, *Phys. B (Amsterdam)* **256-258**, 182 (1998).  
[27] M. Pustilnik and L. Glazman, *J. Phys.: Condens. Matter* **16**, R513 (2004).  
[28] I. V. Borzenets, J. Shim, J. C. H. Chen, A. Ludwig, A. D. Wieck, S. Tarucha, H.-S. Sim, and M. Yamamoto, *Nature (London)* **579**, 210 (2020).  
[29] N. Néel, J. Kröger, R. Berndt, T. O. Wehling, A. I. Lichtenstein, and M. I. Katsnelson, *Phys. Rev. Lett.* **101**, 266803 (2008).

- [30] A. Zhao, Q. Li, L. Chen, H. Xiang, W. Wang, S. Pan, B. Wang, X. Xiao, J. Yang, J. G. Hou, and Q. Zhu, *Science* **309**, 1542 (2005).
- [31] A. Kaminski, Y. V. Nazarov, and L. I. Glazman, *Phys. Rev. B* **62**, 8154 (2000).
- [32] H. R. Krishna-murthy, J. W. Wilkins, and K. G. Wilson, *Phys. Rev. B* **21**, 1003 (1980).
- [33] O. Sakai, Y. Shimizu, and T. Kasuya, *J. Phys. Soc. Jpn.* **58**, 3666 (1989).
- [34] T. Costi and A. Hewson, *Phys. B (Amsterdam)* **163**, 179 (1990).
- [35] T. A. Costi, J. Kroha, and P. Wölfle, *Phys. Rev. B* **53**, 1850 (1996).
- [36] J. Kroha and P. Wölfle, *J. Phys. Soc. Jpn.* **74**, 16 (2005).
- [37] T. A. Costi and A. C. Hewson, *Philos. Mag. B* **65**, 1165 (1992).
- [38] Ph. Nozières and A. Blandin, *J. Phys. (Paris)* **41**, 193 (1980).
- [39] J. Gan, N. Andrei, and P. Coleman, *Phys. Rev. Lett.* **70**, 686 (1993).
- [40] V. J. Emery and S. Kivelson, *Phys. Rev. B* **46**, 10812 (1992).
- [41] J. Gan, *J. Phys.: Condens. Matter* **6**, 4547 (1994).
- [42] A. M. Tsvelick and P. B. Wiegmann, *Z. Phys. B: Condens. Matter* **54**, 201 (1984).
- [43] A. M. Tsvelick and P. B. Wiegmann, *J. Stat. Phys.* **38**, 125 (1985).
- [44] O. Parcollet and A. Georges, *Phys. Rev. Lett.* **79**, 4665 (1997).
- [45] T. Kimura and S. Ozaki, *J. Phys. Soc. Jpn.* **86**, 084703 (2017).
- [46] D. Bensimon, A. Jerez, and M. Lavagna, *Phys. Rev. B* **73**, 224445 (2006).
- [47] D. L. Cox and M. Jarrell, *J. Phys.: Condens. Matter* **8**, 9825 (1996).
- [48] I. Affleck and A. W. Ludwig, *Nucl. Phys. B* **360**, 641 (1991).
- [49] P. Coleman, L. B. Ioffe, and A. M. Tsvelik, *Phys. Rev. B* **52**, 6611 (1995).
- [50] S. Yasui and K. Sudoh, *Phys. Rev. C* **88**, 015201 (2013).
- [51] K. Hattori, K. Itakura, S. Ozaki, and S. Yasui, *Phys. Rev. D* **92**, 065003 (2015).
- [52] L. Fritz and M. Vojta, *Rep. Prog. Phys.* **76**, 032501 (2013).
- [53] A. Principi, G. Vignale, and E. Rossi, *Phys. Rev. B* **92**, 041107(R) (2015).
- [54] A. K. Mitchell and L. Fritz, *Phys. Rev. B* **92**, 121109(R) (2015).
- [55] S. Yasui and K. Sudoh, *Phys. Rev. C* **95**, 035204 (2017).
- [56] S. Yasui, *Phys. Rev. C* **93**, 065204 (2016).
- [57] A. Mukherjee and S. Lal, *Nucl. Phys. B* **960**, 115170 (2020).
- [58] A. Mukherjee and S. Lal, *Nucl. Phys. B* **960**, 115163 (2020).
- [59] A. Mukherjee and S. Lal, *New J. Phys.* **22**, 063007 (2020).
- [60] A. Mukherjee and S. Lal, *New J. Phys.* **22**, 063008 (2020).
- [61] S. Pal, A. Mukherjee, and S. Lal, *New J. Phys.* **21**, 023019 (2019).
- [62] S. Patra and S. Lal, *Phys. Rev. B* **104**, 144514 (2021).
- [63] A. Mukherjee, S. Patra, and S. Lal, *J. High Energy Phys.* **04** (2021) 148.
- [64] G. Yoo, S.-S. B. Lee, and H.-S. Sim, *Phys. Rev. Lett.* **120**, 146801 (2018).
- [65] A. Mukherjee and S. Lal, [arXiv:2003.06118](https://arxiv.org/abs/2003.06118).
- [66] E. S. Sørensen, M.-S. Chang, N. Laflorencie, and I. Affleck, *J. Stat. Mech.: Theory Exp.* (2007) P08003.
- [67] E. Eriksson and H. Johannesson, *Phys. Rev. B* **84**, 041107(R) (2011).
- [68] S.-S. B. Lee, J. Park, and H.-S. Sim, *Phys. Rev. Lett.* **114**, 057203 (2015).
- [69] V. Barzykin and I. Affleck, *Phys. Rev. B* **57**, 432 (1998).
- [70] V. Barzykin and I. Affleck, *J. Phys. A: Math. Gen.* **32**, 867 (1999).
- [71] C. Yang and A. E. Feiguin, *Phys. Rev. B* **95**, 115106 (2017).
- [72] G. Vidal and R. F. Werner, *Phys. Rev. A* **65**, 032314 (2002).
- [73] A. Bayat, P. Sodano, and S. Bose, *Phys. Rev. B* **81**, 064429 (2010).
- [74] N. Andrei and V. T. Rajan, *J. Appl. Phys. (Melville, NY)* **53**, 7933 (1982).
- [75] L. N. Oliveira and J. W. Wilkins, *Phys. Rev. Lett.* **47**, 1553 (1981).
- [76] J. B. Boyce and C. P. Slichter, *Phys. Rev. Lett.* **32**, 61 (1974).
- [77] J. Nygård, D. H. Cobden, and P. E. Lindelof, *Nature (London)* **408**, 342 (2000).
- [78] B. Babić, T. Kontos, and C. Schönenberger, *Phys. Rev. B* **70**, 235419 (2004).
- [79] S. J. Chorley, M. R. Galpin, F. W. Jayatilaka, C. G. Smith, D. E. Logan, and M. R. Buitelaar, *Phys. Rev. Lett.* **109**, 156804 (2012).
- [80] H. C. Manoharan, C. P. Lutz, and D. M. Eigler, *Nature (London)* **403**, 512 (2000).
- [81] G. A. Fiete and E. J. Heller, *Rev. Mod. Phys.* **75**, 933 (2003).
- [82] E. Rossi and D. K. Morr, *Phys. Rev. Lett.* **97**, 236602 (2006).
- [83] H. Prüser, M. Wenderoth, P. E. Dargel, A. Weismann, R. Peters, T. Pruschke, and R. G. Ulbrich, *Nat. Phys.* **7**, 203 (2011).
- [84] A. K. Mitchell, M. Becker, and R. Bulla, *Phys. Rev. B* **84**, 115120 (2011).
- [85] T. A. Costi, *Phys. Rev. Lett.* **85**, 1504 (2000).
- [86] A. Rosch, T. A. Costi, J. Paaske, and P. Wölfle, *Phys. Rev. B* **68**, 014430 (2003).
- [87] B. Groisman, S. Popescu, and A. Winter, *Phys. Rev. A* **72**, 032317 (2005).
- [88] K. Seki and S. Yunoki, *Phys. Rev. B* **96**, 085124 (2017).
- [89] K.-S. Kim, S. B. Chung, C. Park, and J.-H. Han, *Phys. Rev. D* **99**, 105012 (2019).
- [90] V. Berezinskii, *Sov. Phys. JETP* **32**, 493 (1971).
- [91] J. Kosterlitz and D. J. Thouless, *Prog. Low Temp. Phys.* **7**, 371 (1978).
- [92] P. Phillips, *Advanced Solid State Physics* (Cambridge University Press, Cambridge, UK, 2012).
- [93] P. Coleman, *Introduction to Many-Body Physics* (Cambridge University Press, Cambridge, UK, 2015), Chap. 18.
- [94] A. C. Hewson, *The Kondo Problem to Heavy Fermions* (Cambridge University Press, Cambridge, UK, 1993).
- [95] D. C. Langreth, *Phys. Rev.* **150**, 516 (1966).
- [96] P. W. Anderson, *Phys. Rev. Lett.* **18**, 1049 (1967).
- [97] K. Yamada and K. Yosida, *Prog. Theor. Phys.* **59**, 1061 (1978).
- [98] J. Langer and V. Ambegaokar, *Phys. Rev.* **121**, 1090 (1961).
- [99] R. M. Martin, *Phys. Rev. Lett.* **48**, 362 (1982).
- [100] S. Fujimoto and N. Kawakami, *J. Phys. Soc. Jpn.* **66**, 2157 (1997).
- [101] R. Shiina and C. Ishii, *J. Low Temp. Phys.* **91**, 105 (1993).
- [102] C. Lacroix and M. Cyrot, *Phys. Rev. B* **20**, 1969 (1979).
- [103] S. Burdin, D. R. Grempel, and A. Georges, *Phys. Rev. B* **66**, 045111 (2002).
- [104] J. Rech, P. Coleman, G. Zarand, and O. Parcollet, *Phys. Rev. Lett.* **96**, 016601 (2006).